Ilpo Weijola

Solar Panel Applications and Their Simulation

Metropolia University of Applied Sciences

Bachelor of Engineering

Degree Programme in Electronics

Bachelor's Thesis

8 September 2022

Abstract

Author:	Ilpo Weijola
Title:	Solar Panel Applications and Their Simulation
Number of Pages:	58 pages
Date:	8 September 2022
Degree:	Bachelor of Engineering
Degree Programme:	Degree Programme in Electronics
Professional Major:	Electronics
Supervisor:	Janne Mäntykoski, Senior Lecturer

Solar power has become one of the most established forms of more environmentally sustainable alternative energy production, and it has been the most widely applied in small-power systems, such as off-grid power production units. Computer assisted simulation of such systems is a powerful tool in facilitating their design and implementation. A complication in the simulation is that the performance of solar cells is very strongly dependent on environmental conditions such as temperature and irradiance.

Focusing on the design of affordable and efficient solar power applications, this study looks into the analysis and simulation of individual solar cells as well as entire solar panel based systems. These considerations are then supplemented by taking real-world operating conditions of solar power applications into account.

Simulation and programming of methods that assist in tasks such as impedance matching and maximum power point tracking are highlighted as important advances in the implementation of solar panel based systems.

In conclusion, solar panel applications are an efficient and reliable method for small-scale energy production and simulation greatly facilitates the design of such systems.

Keywords: solar power, alternative energy, green energy, MPPT

Tiivistelmä

Tekijä: Ilpo Weijola
Otsikko: Aurinkopaneelien sovellukset ja niiden simulointi
Sivumäärä: 58 sivua
Aika: 8.9.2022

Tutkinto: Insinööri (AMK)
Tutkinto-ohjelma: Degree Programme in Electronics
Ammatillinen pääaine: Electronics
Ohjaaja: Lehtori Janne Mäntykoski

_____

Aurinkoenergiasta on tullut yksi vakiintuneimmista vaihtoehtoisen ympäristötietoisen energian tuotantomuodoista, ja sen pääasialliset sovelluskohteet ovat olleet pienitehoisissa järjestelmissä, kuten yleisestä sähköverkosta erillisissä energiantuotantoyksiköissä. Tällaisten järjestelmien tietokoneavusteinen simulointi helpottaa olennaisesti niiden suunnittelua ja käyttöä. Simulointia hankaloittaa se, että aurinkokennojen toiminta on voimakkaasti riippuvaista ympäristöolosuhteista, kuten lämpötilasta ja säteilytysvoimakkuudesta.

Tässä tutkielmassa perehdytään sekä yksittäisten aurinkokennojen että kokonaisten aurinkopaneelijärjestelmien analysointiin ja simulointiin. Näitä aiheita täydennetään ottamalla huomioon sellaiset todellisen maailman olosuhteet, joissa aurinkoenergiajärjestelmien on kyettävä toimimaan. Tärkeitä edistysaskelia aurinkopaneelijärjestelmien soveltamisessa käytäntöön ovat simulointi sekä sellaisten menetelmien ohjelmointi, jotka parantavat aurinkopaneelijärjestelmän hyötysuhdetta edesauttamalla muun muassa impedanssisovitusta tai maksimitehopisteen seurantaa.

Johtopäätöksenä voidaan esittää, että aurinkopaneeleihin perustuvat sovellukset ovat tehokas ja luotettava pienen mittakaavan energiantuotannon menetelmä ja simulointi helpottaa tällaisten järjestelmien suunnittelua huomattavasti.

Avainsanat: aurinkoenergia, vaihtoehtoinen energia, puhdas energia, maksimitehopisteen seuranta

Contents

List of Abbreviations

IGBT: Insulated Gate Bipolar Transistor

LabVIEW: Laboratory Virtual Instrument Engineering Workbench

MOSFET: Metal Oxide Semiconductor Field Effect Transistor

MPPT: Maximum Power Point Tracking

PWM: Pulse Width Modulation

P&O: Perturb and Observe

1 Introduction

Some substances, particularly metals, are susceptible to having electrons of their atoms dislocated by incoming energy in the form of light. This effect can be harnessed in a device known as a photoelectric cell in order to create a photoelectric voltage that can be used in different applications. Historically, photoelectric cells have been characterized by low power output on the one hand, but on the other hand an instantaneous response to differences in the conditions in which they are exposed to illumination. This has made them particularly useful in applications such as television cameras, automatic manufacturing process controls, door openers, and burglar alarms. [1, 40-41.]

Throughout the development of photoelectric cell technology, one particular application involving the use of this technology in supplying power has been of considerable interest. This is the development of devices known as solar cells, namely, semiconductor devices that convert sunlight directly into electric current to produce usable electric power as long as there is light shining on them. [2, 382.]

In what follows, the main concerns will be the dependence of the operation of the solar cells on environmental factors (mainly temperature) as well as matching the solar cell output to the load. In addition, mathematical models to represent solar cell operation and different computer-assisted methodologies to increase the solar cell power output will be considered. The ultimate goal is to design the basics of an affordable and efficient solar power application, presumably for small-scale off-grid applications, due to this being the predominant market for alternative energy based microgeneration systems. Solar cells have become popular in low-power applications for residential buildings such as summer cottages.

Given the abundance of electrical devices that are capable of operating with low-voltage direct current, it may not be necessary to even convert the output of

a solar cell into the type of high-voltage alternating current electricity that is available from the national electrical grid network. Depending on the requirements presented by the load, however, it may be necessary to utilize a direct current to direct current voltage converter, possibly with microcontroller-assisted operation [3, 168-179]. Another factor to consider is the fact that shaded solar cells will exhibit severe deterioration of their performance [4, 196].

A solar power system can be supplemented with other renewable forms of energy, such as wind power. Since it is seldom sunny during windy weather, wind power in particular offers advantages considering the reliability of the availability of electrical power [3, 165].

2   Basic Operation of Solar Cells

A conventional solar cell consists of a relatively thin n-type region (order of 1 µm, also referred to as the emitter) and a relatively thick p-type region (order of 300 µm, also referred to as the base), which are made of semiconductor materials [2, 384-385]. A schematic of a conventional solar cell is shown in figure 1 below. Sunlight falling on the solar cell results in a photocurrent being generated and flowing through the external load (light bulb in figure 1). The work done by this current flow can be harnessed and converted into a useful form (such as the illuminating power of the light bulb in figure 1). [2, 386; 5.]
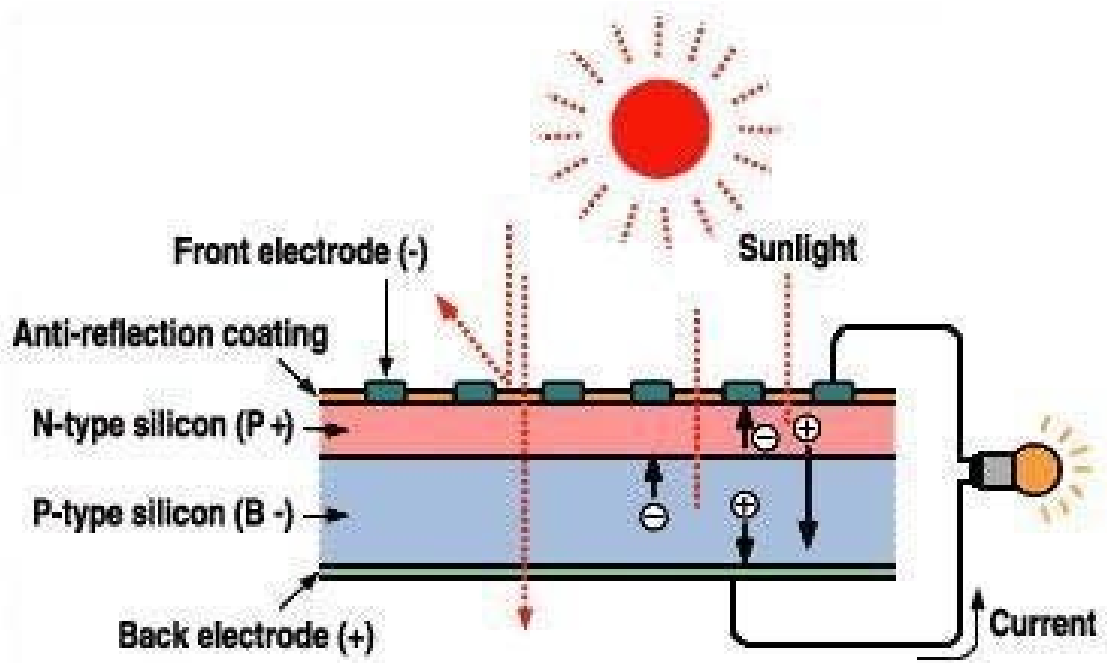
Figure 1. Basic schematic of a solar cell [5].

A basic figure describing the operation of a solar cell is the I-V curve. This is shown in figure 2 below. Figure 2 also plots the power produced by the cell and shows the maximum power point P_{MP}, namely the point where the product of the local current and the local voltage values is the greatest. At the maximum power point, the voltage is designated V_{MP} and the current is designated I_{MP} in Figure 2. [6.]

The I-V curve is limited, on the one hand, by the short circuit current, also known as photocurrent, of the solar cell, designated I_{SC} in figure 2. This is the photogenerated current that would flow in the circuit containing the solar cell if there were no external load. On the other hand, the I-V curve is limited by the open circuit voltage V_{OC}, which, as the name suggests, is the difference in potential that would be produced between the two ends of the solar cell if there were nothing at all connected to it. [6.]

The power curve in a graph such as figure 2 is obtained simply by multiplying each momentary voltage value with the corresponding momentary current value

that is plotted on the I-V curve. Therefore, the power curve begins at zero watts (at the short circuit current, i.e., when the voltage is zero) and ends at zero watts (when the current reaches zero). This means that anything that influences the I-V curve will inevitably influence the power curve as well. Power being the product of voltage and current is indicated in figure 2 alongside the power curve. [6.]
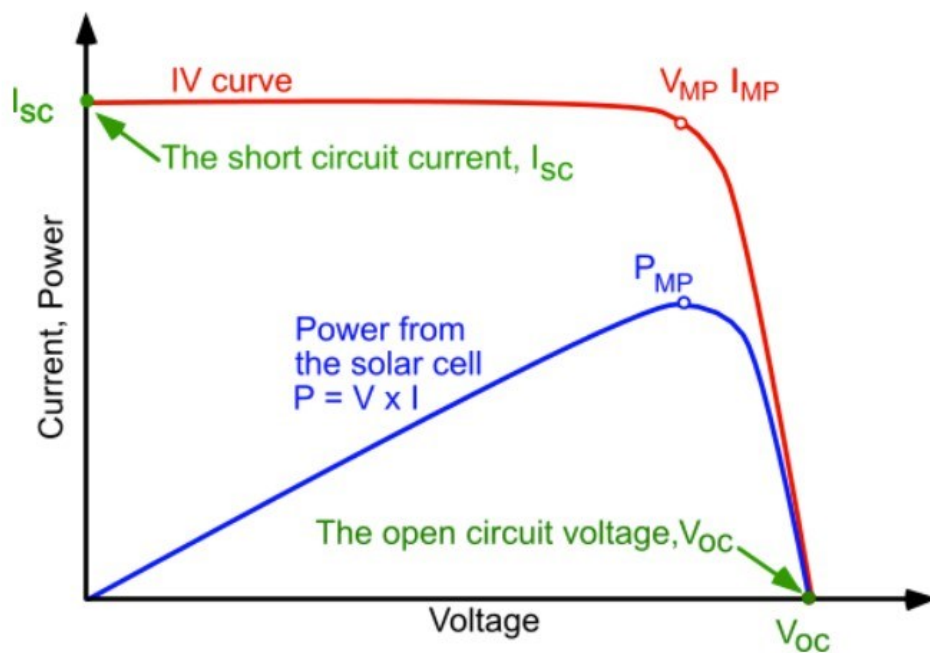

Figure 2. An example I-V curve of a conventional solar cell. The determination of the maximum power point is also shown. [6.]

There are two possible ways to arrive at the I-V curve presented in figure 2 above. One way is to experimentally measure the output voltage and the output current of a consistently illuminated solar cell as the external load connected to it has its value varied from zero ohms to several kiloohms. The other way is to mathematically formulate the I-V curve based on the fundamental equations of semiconductor physics that govern the operation of any solar cell. The I-V curve and the power curve, such as the ones presented in figure 2, are always obtained under constant irradiance and in constant temperature. [2, 465-466.]

For the reasons expressed above, it is best that a procedure such as maximum power point tracking (MPPT) is not thought of as a method to reach the maximum power point on a static power curve such as the one in figure 2. In a real-world application, particularly in the case of impedance matching being involved, the load may not vary considerably, whereas the factors that are kept constant in a standard laboratory measurement where the I-V and power curves are determined may be subject to extremely rapid and dramatic shifts. These factors include the previously mentioned ones, namely temperature and irradiance, as well as other, possibly related, factors such as shading (insects may fly close to the solar panels), etc. [3, 165-174.]
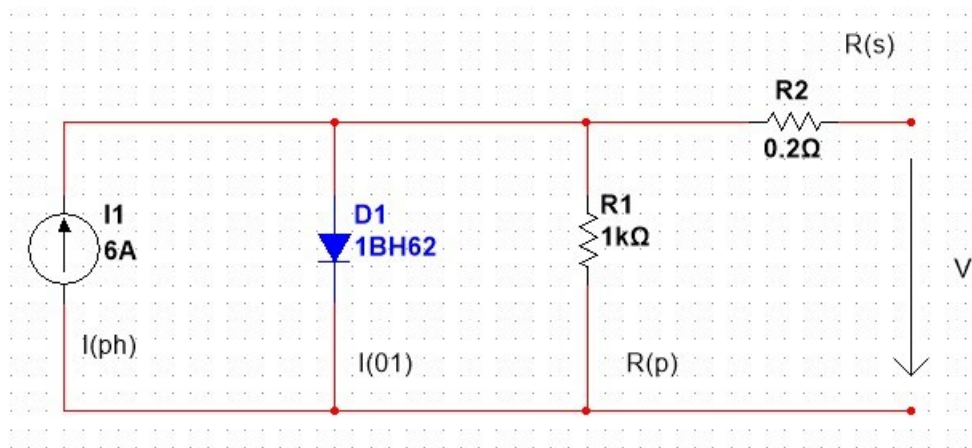

Figure 3. A one-diode equivalent circuit model for a solar cell with example values for I1, R1, and R2. Made with National Instruments MultiSim software.

There is a considerable number of different electrical equivalent circuit models or mathematical models for solar cells available in the literature. Let us concentrate on a fairly simplified equivalent circuit model as described in figure 3. The equation describing this model of solar cell operation is:

$$I = I_{SC} - I_0 \left(e^{\left(\frac{q(V+IR_S)}{nkT} \right)} - 1 \right) - \frac{V+IR_S}{R_p} \tag{1}$$

Where I is the output current of the solar cell, I_{SC} is the photocurrent of the solar cell, I_0 is the saturation current from base (p-silicon) and emitter (n-silicon), q is the electron charge ($1.6012\text{x}10^{-19}$ C or 1 eV), V is the output voltage of the solar cell, n is a dimensionless diode factor, k is Boltzmann's constant ($8.617\text{x}10^{-5}$ eV/K), T is the temperature in Kelvin and, finally, R_s and R_p are the series and parallel resistances, respectively, as presented in figure 3. [7, 216; 8.]

The series resistance (R_s in equation 1) arises from the bulk resistance of the semiconductor and the resistance of contacts and interconnection. Series resistance is a particular problem at high current, for instance, under concentrated light. The parallel resistance (R_p in equation 1) arises from leakage current around the edges of the solar cell and extended lattice defects in the depletion region. For an efficient solar cell, the series resistance should be as small as possible, whereas the parallel resistance should be as large as possible. [2, 479.]

Considering that the primary focus in the current analysis lies in the dependence of solar cell operation on the temperature T as well as the irradiance G, the equation for the photocurrent I_{SC} turns out to be worth a thorough examination:

$$I_{SC} = I_{SC,STC}\frac{G}{G_{STC}}\left(1 + \alpha_1\left(T_{PV} - T_{PV,STC}\right)\right) \qquad (2)$$

Where $I_{SC,STC}$ and G_{STC} refer to the photocurrent and the irradiance, respectively, in standardized test conditions. The irradiance under standardized test conditions is generally considered to be 1000 W/m^2. T_{PV} is the solar cell temperature and $T_{PV,STC}$ is the solar cell temperature under standardized test conditions, as expected. The temperature under standardized test conditions is generally considered to be 25 °C. α_1 is temperature coefficient of the photocurrent. The values for $I_{SC,STC}$ and α_1 are customarily provided in the solar cell data sheet. [7, p.215, 217.]

Another term in equation 1 that requires scrutiny is the saturation current I_0. This is the short circuit current that would flow through the solar cell if there were no illumination falling on the solar cell, i.e., if the solar cell was left in the dark [2, 464-465]. Despite being one of the fundamental terms in the equations governing the operation of a solar cell, this saturation current cannot be inferred from the I-V curve, because the I-V curve is always obtained under standardized test irradiance conditions.

Equations 1 and 2 have been formulated based on the fundamental semiconductor physics that governs the operation of a solar cell. After considerable algebra and approximations, equations for both the voltage and the current at the maximum power point of the I-V curve can be presented. In accordance with basic laws of electrical phenomena, the maximum power obtainable can then be determined by simply multiplying together these voltage and current values obtained at the maximum power point. [2, 467.]

The approximate equation for the voltage at the maximum power point in terms of the open circuit voltage V_{OC} is:

$$V_{MP} \approx V_{OC} - \frac{kT}{q} ln \left(\frac{qV_{OC}}{kT} + 1 \right) \tag{3}$$

Whereas the approximate equation for the current at the maximum power point in terms of the photocurrent I_{SC}, the saturation current I_0, and the open circuit voltage V_{OC} is:

$$I_{MP} \approx I_{SC} - I_0 e^{\left[\frac{q}{kT} V_{OC} - ln \left(\frac{qV_{OC}}{kT} + 1 \right) \right]} \tag{4}$$

In equations 3 and 4 above, k is Boltzmann's constant (8.617×10^{-5} eV/K), T is the temperature in Kelvin, and q is the electron charge (1.6012×10^{-19} C or 1 eV). Equations 3 and 4 make the approximation of the maximum power point as well as, through multiplication of the obtained voltage and current values, the approximation of the obtained maximum power possible if the open circuit

voltage V_{OC} and the short circuit and saturation currents I_{SC} and I_0 are known. [2, 467.]

Figure 4 below presents the same one-diode model of a solar cell as in figure 3 above, except that an external load resistor R3 has been added. As will be shown, when the value of this load resistor is swept from zero ohms to four ohms, the basic shapes of the voltage, current and power curves for a solar cell can be obtained by plotting the voltage across the load resistor, the current through the load resistor, and the power dissipated in the load resistor, respectively, as function of the load resistance. The following simulations were conducted, and the graphs obtained with the National Instruments MultiSim software. Due to the complicated nature of the calculations necessary to obtain the I-V curve, it cannot be readily obtained using circuit simulation software such as MultiSim.
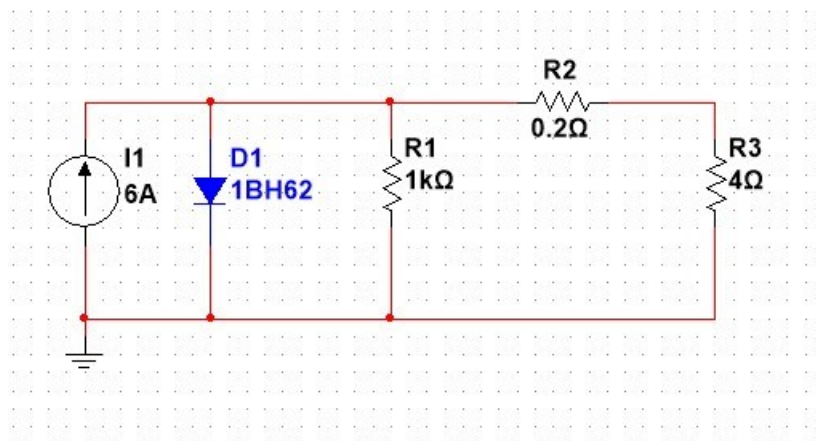

Figure 4. The one-diode model of a solar cell presented with load resistor R3. Made with National Instruments MultiSim software.

Figure 5 shows the voltage drop in the load resistor R3 in figure 4 as a function of the resistance of that load resistor. By interpreting figure 5, it is discovered that the one-diode model of a solar cell presented in figures 3 and 4 has an open circuit voltage of approximately 1.55 volts.
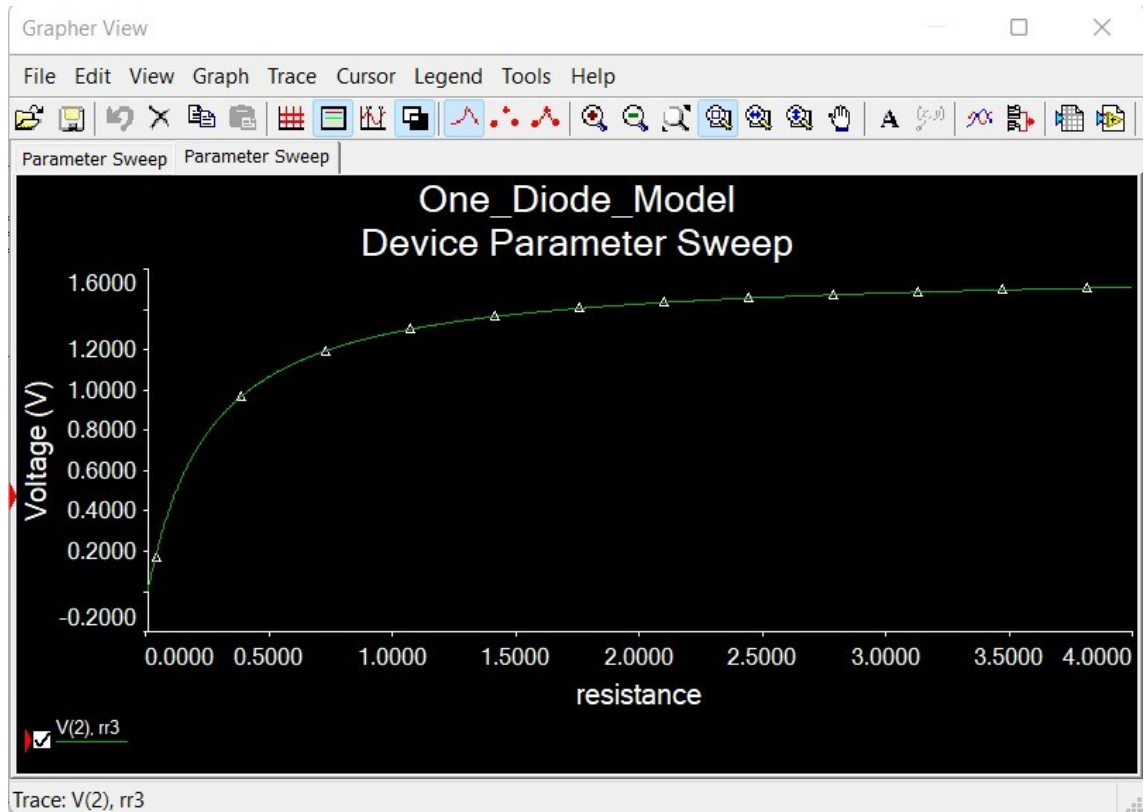
Figure 5. Output voltage of one diode solar cell model plotted against load resistance with MultiSim.

Figure 6 shows the graph of the current through the load resistor in figure 4. The value of the current source in figures 3 and 4 determines the short circuit current at a load resistance of zero ohms, and from there on the current graph exemplifies the typical shape of the current graph of a solar cell as the load resistance value increases.
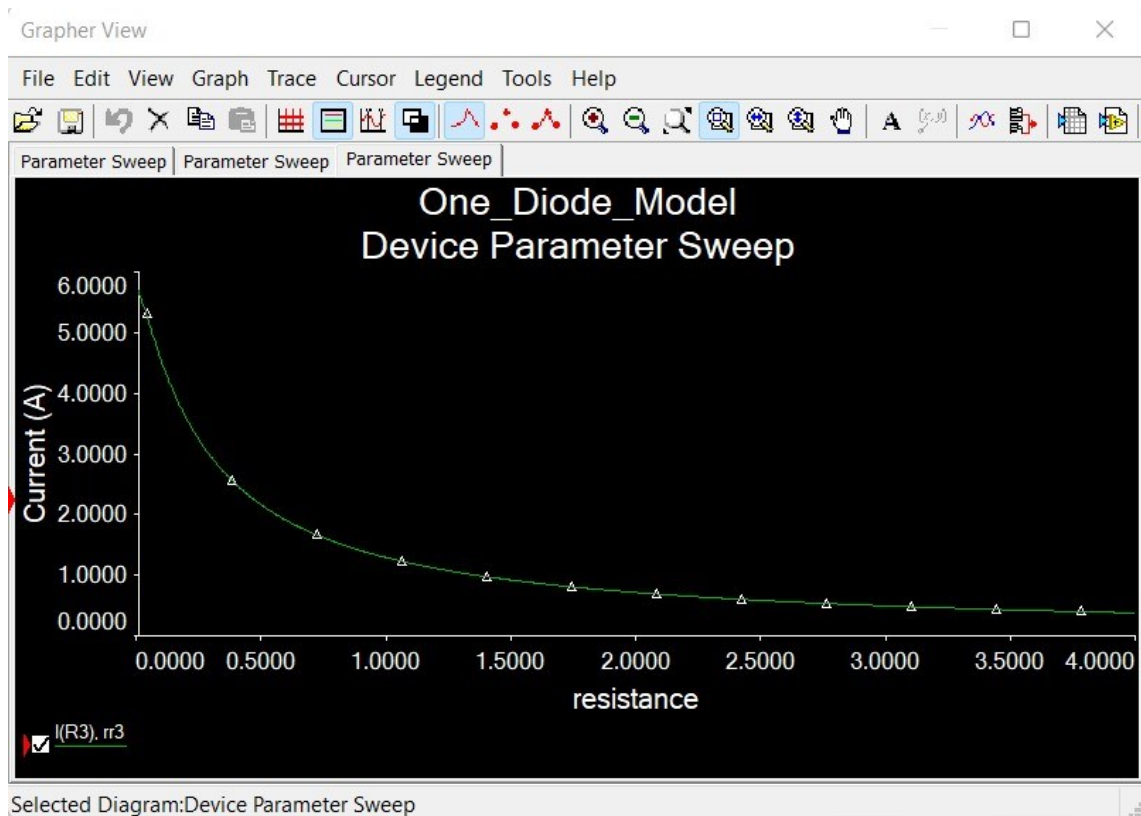
Figure 6. Output current of one diode solar cell model plotted against load resistance with MultiSim.

Figure 7 shows the final basic curve, namely the power graph, of the circuit presented in figure 4 as a function of the load resistance. The maximum power obtainable from this solar cell model turns out to be approximately 2.5 watts at a load resistance slightly less than half an ohm.
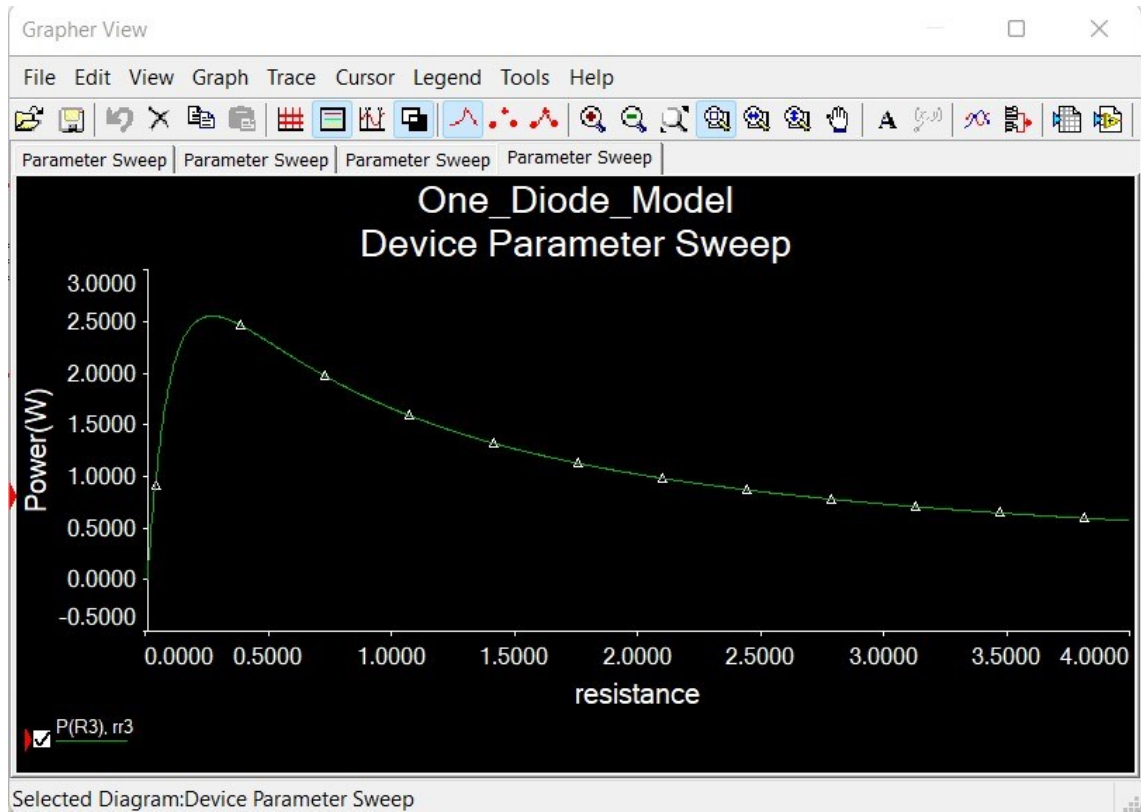
Figure 7. Output power of one diode solar cell model plotted against load resistance with MultiSim.

Finally, figure 8 below plots the voltage, current, and power graphs of figures 5, 6, and 7 together in the same figure. At the maximum power point of 2.5 watts the voltage appears to be approximately one volt, and the current appears to be approximately 2.5 amperes. The product of these voltage and current values is, naturally, 2.5 watts. Also, the resistance at the maximum power point was determined to be slightly less than half an ohm, corresponding to the value of one divided by 2.5, which is what Ohm's law says it should be.
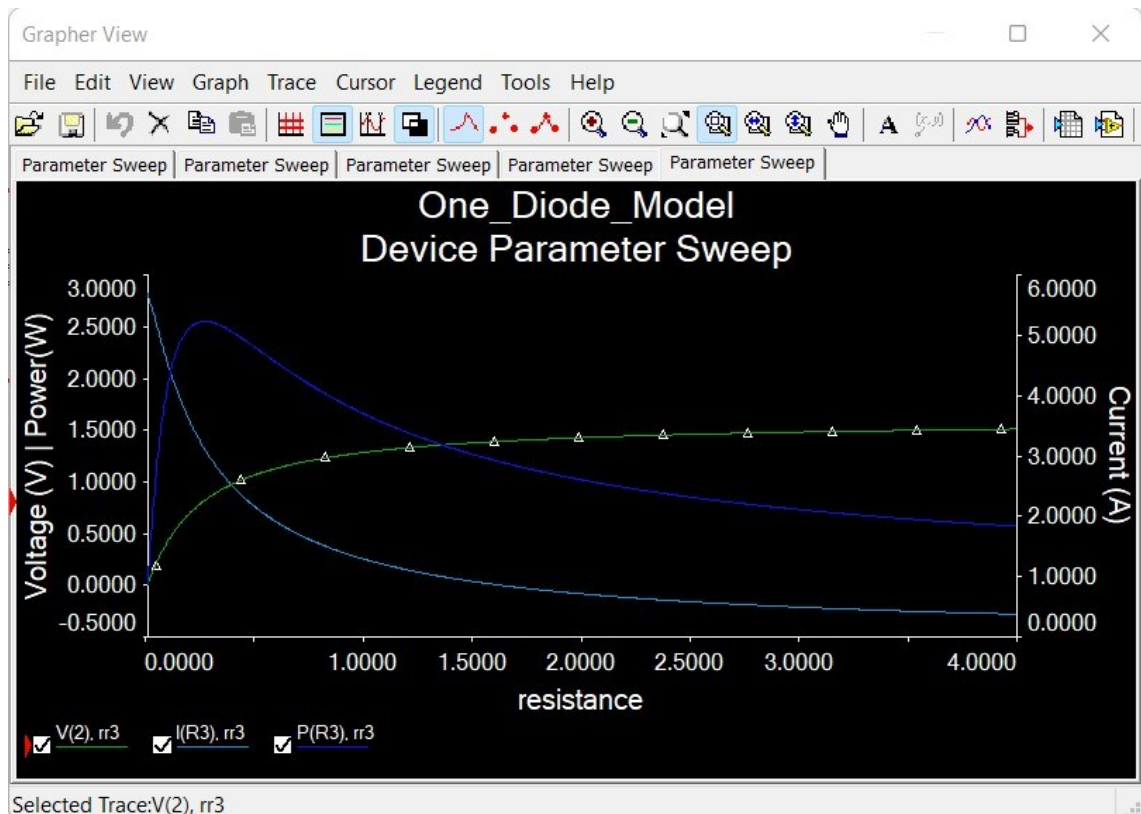
Figure 8. Output voltage (green), current (cyan) and power (blue) of a one diode solar cell model plotted against load resistance with MultiSim.

Next, similar simulation results for a variety of different models of solar cells and solar panels will be considered.

3 Computational Solar Cells and Panels

The diagram presented in figure 4 is that of a one-diode model of a solar cell. There exist some computational models of this approximation of a solar cell, one of which is examined next. The developers of this model have determined its short circuit current I_{SC} to equal 0.034 A and its saturation current I_0 to equal 10^{-11} A [9]. Figure 9 below shows the arrangement in MultiSim. The direct current voltage source that is labelled Virrad in figure 9 corresponds to the value of the irradiance, which has been determined to be at the standardized value of

1000 W/m^2, since one volt corresponds to one watt per square metre in this model.
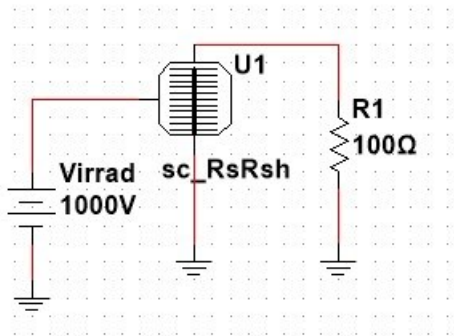

Figure 9. Diagram of computational one-diode solar cell model simulation arrangement in MultiSim.

Figure 10 shows the voltage across the load resistor and the current through the load resistor as functions of the load resistance in the circuit of figure 9. The short circuit current value of 0.034 A is confirmed by the graph in figure 10.
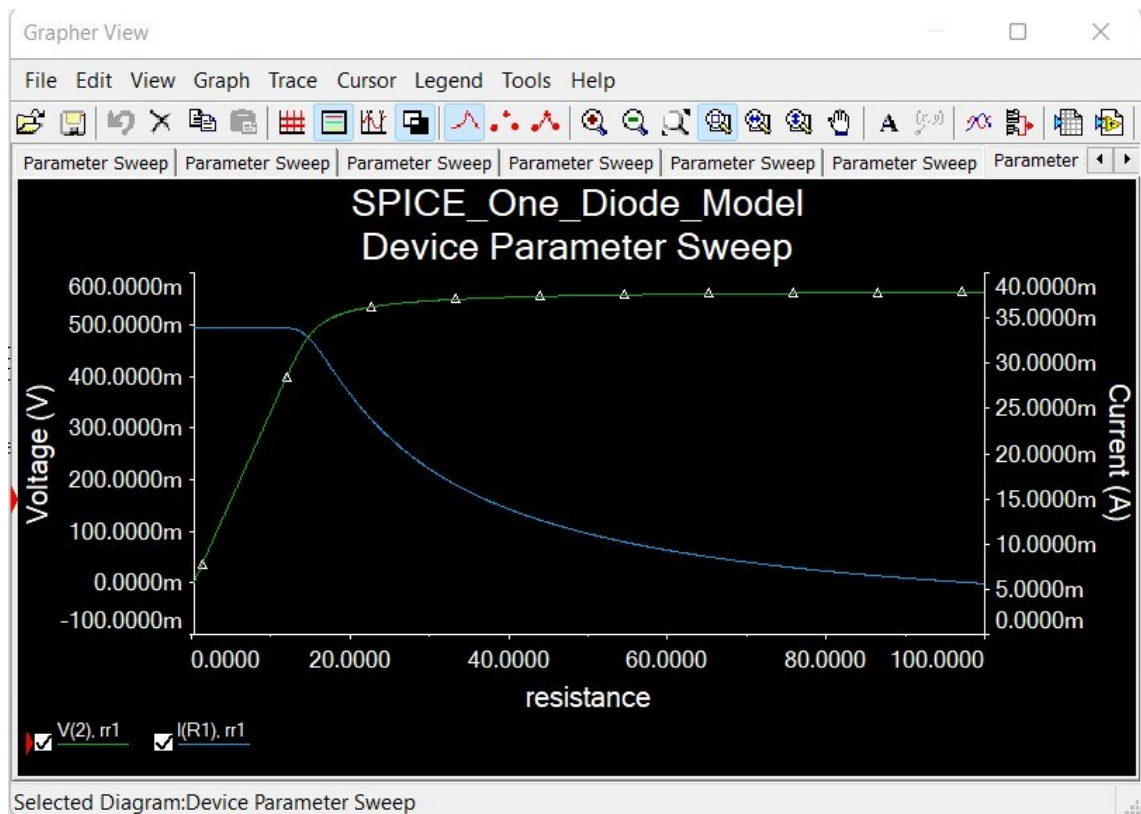

Figure 10. Output voltage (green) and current (cyan) of computational one diode solar cell model plotted against load resistance with MultiSim.

Finally, the power dissipated in the load resistor in the circuit of figure 9 is shown as a function of the load resistance in figure 11 below. The obtainable maximum power from this model appears to be 0.016 W. For the sake of clarity, the power was not plotted to the same graph with the voltage across and the current through the load resistor, but by comparing figures 10 and 11, the output voltage at the maximum power point can be determined to be approximately 0.45 V whereas the output current at the maximum power point can be determined to be approximately 0.032 A. Furthermore, the open circuit voltage V_{OC} of the circuit in figure 9 can be determined to be approximately 0.55 V by looking at figure 10, and the values for the short circuit current I_{SC} at 0.034 A and the saturation current I_0 at 10^{-11} A were already had. By combining this information and substituting it into equations 3 and 4, the voltage and current at the maximum power point can be approximated to be 0.47 V and 0.033 A, respectively. The product of these voltage and current values is approximately 0.0155 W. These values are almost equal to the values determined graphically from figures 10 and 11, so that the equations and models that have been dealt with this far appear to be in good agreement with one another.
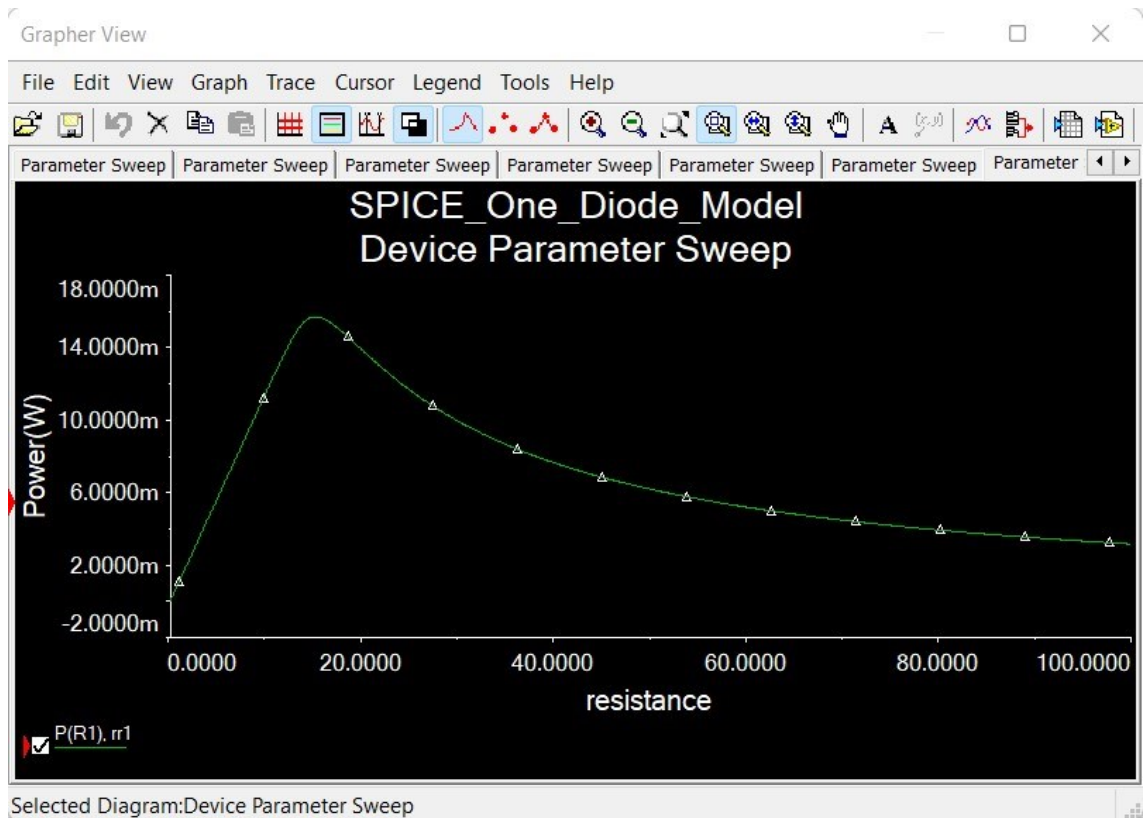
Figure 11. Output power of computational one diode solar cell model plotted against load resistance in MultiSim.

The authors of the one-diode model presented above also provided a model for an entire solar panel with 72 individual solar cells connected in series [9]. The modelling of the operation of a solar panel regarding the temperature and irradiance dependencies will be examined along with this model. The connection, admittedly like the previous MultiSim application that was examined, is presented in figure 12 below.
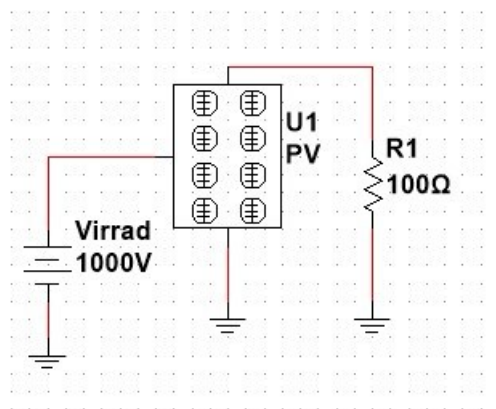

Figure 12. Diagram of computational solar panel model simulation arrangement in MultiSim.

Figure 13 shows the output voltage, output current, and power output characteristics of the solar cell model of figure 12. This time, the maximum power point is achieved with a load resistance of approximately 12 ohms. At the maximum power point, the output voltage is approximately 40 V, and the output current is approximately 3 A. The maximum output power appears to be 120 W, the product of the output voltage and output current values.
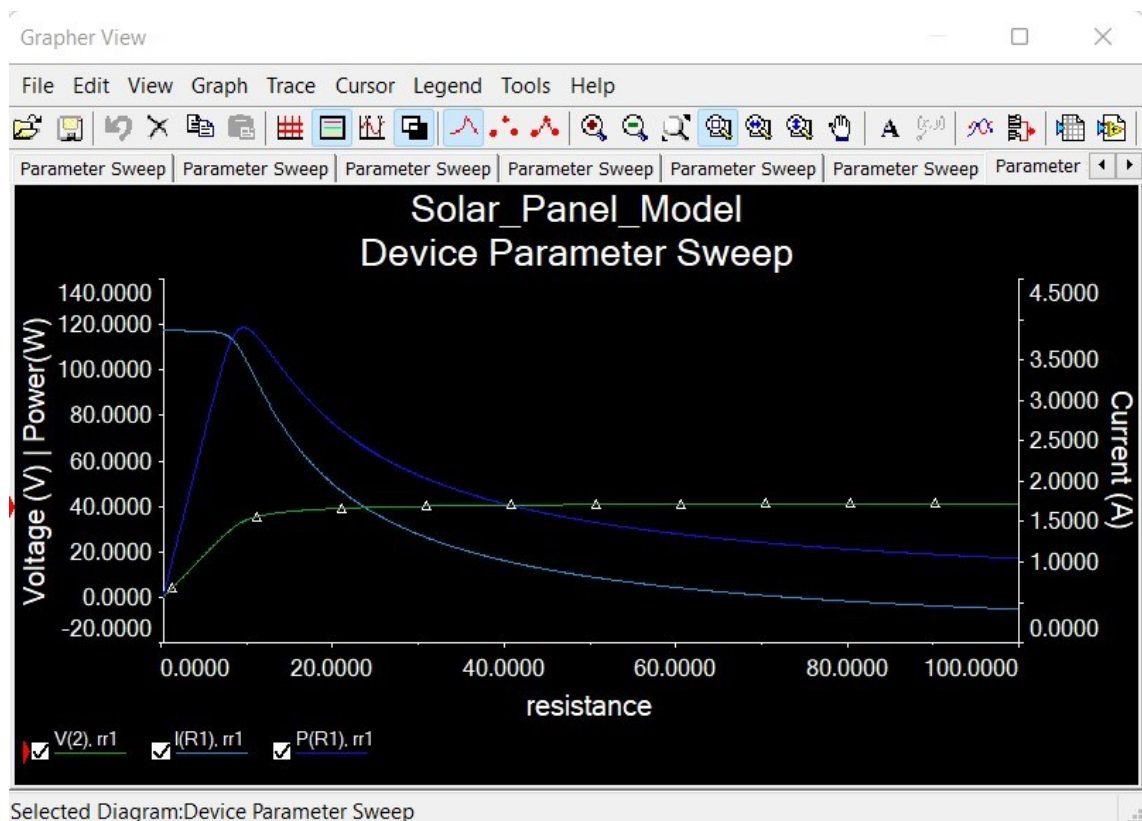

Figure 13. Output voltage (green), current (cyan) and power (blue) of computational solar panel model plotted against load resistance in MultiSim.

Figure 14 shows the output power graph of figure 13 plotted at 11 different temperature values, starting from 0 °C and increasing in steps of 7.5 °C up to a value of 75 °C. In figure 14, the power output always decreases as the temperature increases, so that the highest curve corresponds to the lowest temperature (0 °C) and the lowest curve corresponds to the highest temperature (75 °C). It deserves to be noted that the maximum obtainable power output drops to almost half the value at 0 °C as the temperature rises to 75 °C.
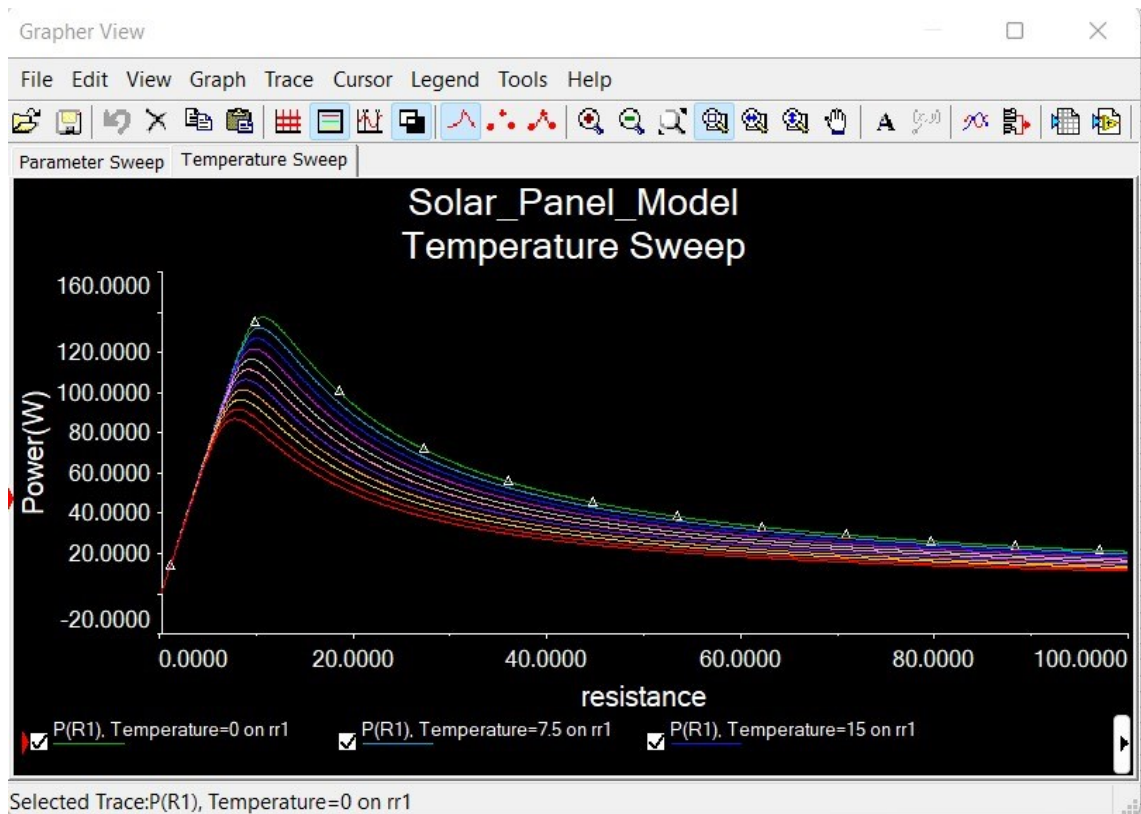
Figure 14. Output power of simulated solar panel model shown in figure 12 plotted against load resistance in 11 different temperatures ranging from 0 °C to 75 °C in steps of 7.5 °C. The power decreases as the temperature increases.

Figure 15 compares the power curve from figure 13 at ten different levels of irradiance, starting from 100 W/m^2 and increasing in steps of 100 W/m^2 until a value of 1000 W/m^2, which has been the standard value used this far. The simulated results presented in figure 15 were obtained in a temperature of 27 °C, which is the standard temperature used in the model that is presently being examined. In figure 15, the considerable impact of the irradiance on the maximum power point should be noted. Naturally, the power output increases with irradiance, so that the lowest power curve corresponds to the lowest irradiance and the highest curve to the highest irradiance.
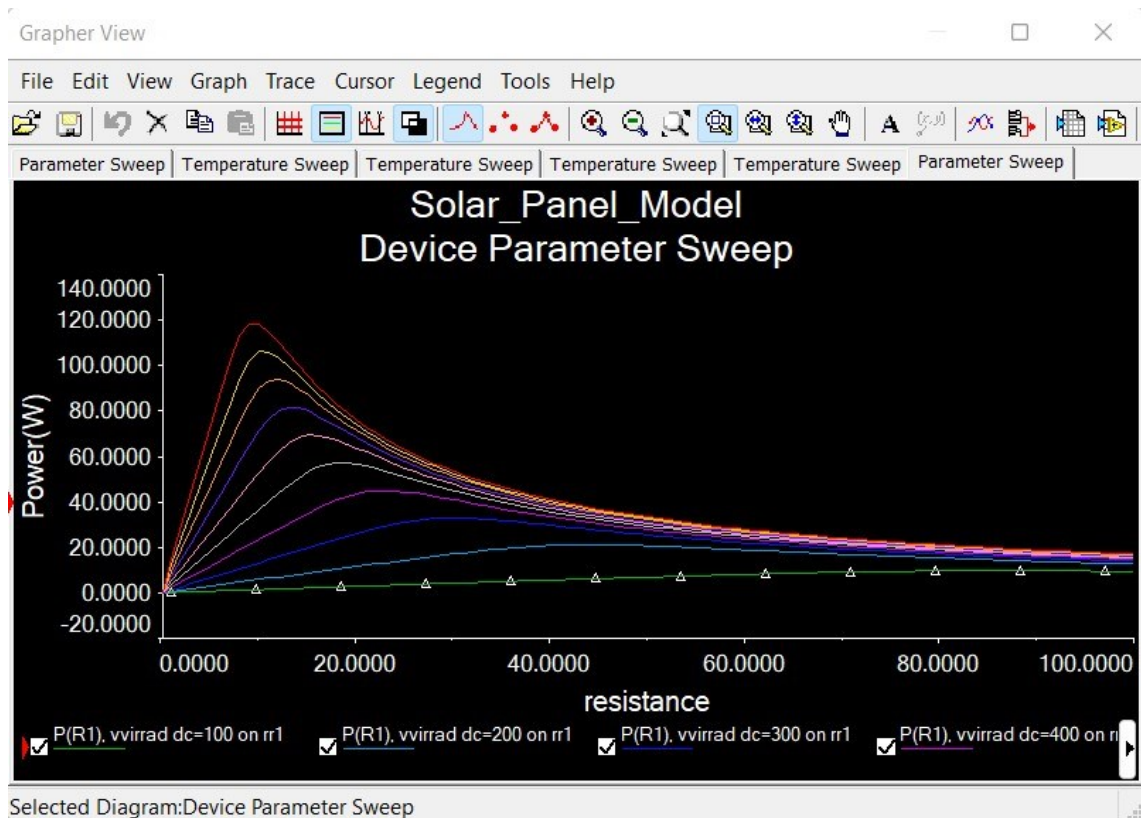
Figure 15. Output power of computational solar panel model shown in figure 12 plotted against load resistance in ten different values of irradiance ranging from 100 W/m^2 to 1000 W/m^2 in steps of 100 W/m^2. The power increases along with the irradiance.

Finally, figure 16 shows the dependence of the simulated results of the solar panel model on both temperature and irradiance. In figure 16, the two highest power curves are obtained at an irradiance of 1000 W/m^2. The temperature values for these two power curves are 0 °C (the highest curve) and 75 °C (the second highest curve). The two lower power curves were obtained at the same temperatures, but with an irradiance of only 333 W/m^2. Naturally, the lowest power curve in figure 16 is the one obtained at an irradiance of 333 W/m^2 in a temperature of 75 °C. The difference in power output is the most pronounced at lower load resistance values, however, the highest curve is still located at approximately twice the power output of the lowest curve as the load resistance increases in figure 16.
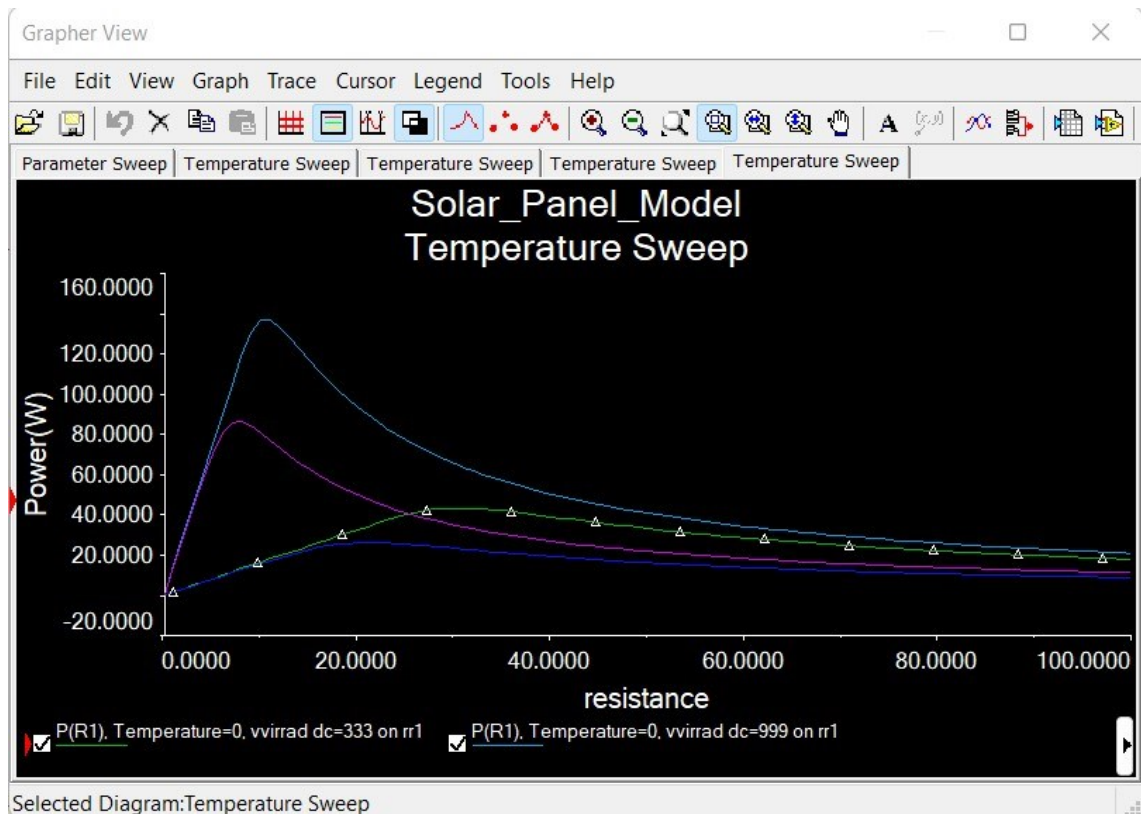
Figure 16. Output power of computational solar panel model shown in figure 12 plotted against load resistance in 0 °C and 1000 W/m^2 (cyan), 75 °C and 1000 W/m^2 (purple), 0 °C and 333 W/m^2 (green), and 75 °C and 333 W/m^2 (blue).

Figure 17 presents another model for an entire solar panel, this time one that is constructed using discrete components in MultiSim. The author of this circuit has provided equations with which the open circuit voltage, the short circuit current as well as both the voltage and the current at the maximum power point can be determined [10]. In figure 17, R3 is the load resistor.
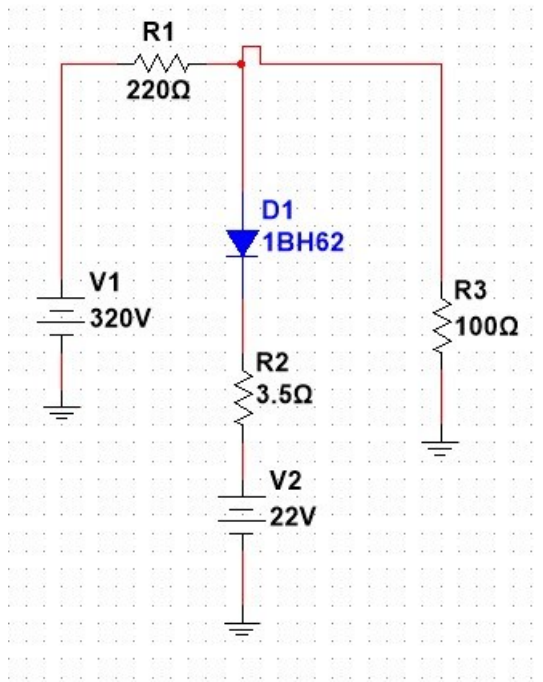
Figure 17. Simulated solar panel model using readily available component models in MultiSim.

The equation for the open circuit voltage of the circuit presented in figure 17 is:

$$V_{OC} = V2 + \left[\frac{R_2}{(R_1+R_2)}\right] \times (V_1 - V_2 - V_\gamma) + V_\gamma \tag{5}$$

The equation for the short circuit current of the circuit presented in figure 17 is:

$$I_{SC} = \frac{V_1}{R_1} \tag{6}$$

The equation for the voltage at the maximum power point is:

$$V_{MP} = V_2 + V_\gamma \tag{7}$$

The equation for the current at the maximum power point is:

$$I_{MP} = \frac{(V_1 - V_{MP})}{R_1} \qquad (8)$$

In equations 5–8, V_1 and V_2 are the values of the direct current voltage sources V1 and V2, 320 V and 22 V, respectively, in figure 17. Similarly, R_1 and R_2 are the values of the resistors R1 (220 Ω) and R2 (3.5 Ω), in figure 17. V_Y is the on voltage of the diode in the model, which, in the case of the diode used in this case (1BH62) is approximated as 1.2 V.

Based on equations 5–8, the open circuit voltage of the model is 27.85 V, the short circuit current of the model is 1.45 A, the voltage at the maximum power point is 23.2 V and the current at the maximum power point is 1.35 A. The product of the voltage at the maximum power point and the current at the maximum power point, which corresponds to the maximum power output, is 31.32 W. These are practically the same values that are determined graphically in figure 18 below.
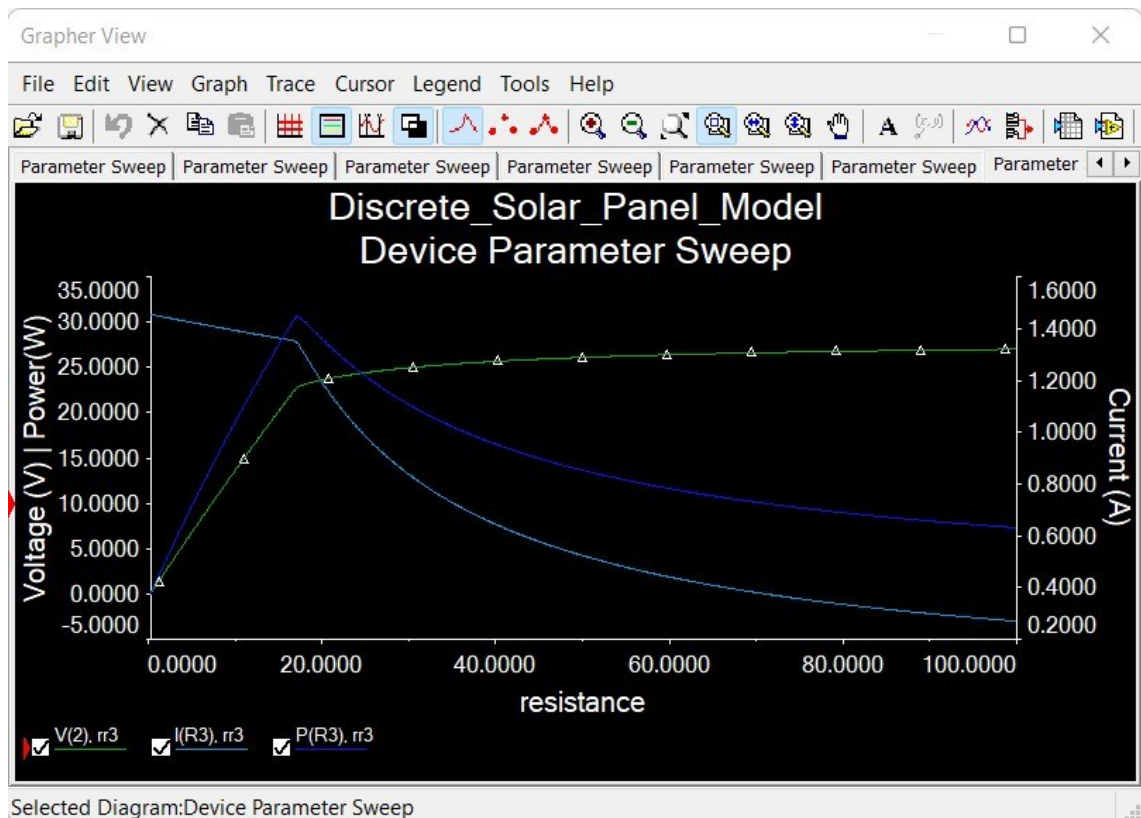
Figure 18. Output voltage (green), current (cyan), and power (blue) of discrete component solar cell model shown in figure 17 plotted against load resistance.

At this point, a view presenting a wider understanding of solar cell and solar panel operation, as well as its dependence on environmental factors, will be adapted.

4   Real-World Practical Considerations

This far, the focus in this study has been on the theoretical modelling of solar cells and panels. However, the importance of taking the environmental conditions into account has already been stressed. Furthermore, various aspects of the real-world performance will depend on the practicalities of any given solar power application. The focus is now shifted onto things that affect the real-world performance of solar power applications. This chapter begins with a brief examination into the physical basis of the temperature dependence of solar cell

performance. This is then followed by investigations into the considerations of impedance matching and tracking the maximum power point that are relevant to real-world applications involving solar power.

4.1   Solar Cell Performance Dependence on Temperature

The thing about the dependence of solar cell efficiency on temperature is that the governing equations that model the functioning of solar cells have various parameters that depend on temperature in themselves. These parameters include band gap energy, diffusion coefficients, diffusion lengths, built-in voltage, depletion region width, and intrinsic carrier concentration. This makes the mathematical modelling of solar cell efficiency on temperature considerably complicated. However, some general guidelines regarding the relationship between solar cell efficiency and temperature can be presented. The graph that shows the efficiency as a function of temperature is generally a linear dependence that is inversely proportional, starting at an efficiency of 0.2 at approximately minus thirty centigrade and linearly decreasing to an efficiency of 0.12 at approximately plus ninety centigrade. [2, 478.]

4.1.1 Band Gap Energy

A very crude explanation of band gap energy is that it is a measure of the amount of energy that is needed to be introduced to a system of particular atoms in order to produce an electron-hole pair in the material. For silicon, the band gap energy is approximately 1.125 electron volts. This means that as the solar cell is hit by light, photons that have greater energy than this will cause the solar cell to work. [2, p.385, 406-407.]

4.1.2 Diffusion Coefficients

In considering a silicon crystal lattice, it is important to note that electrons in the lattice cannot really be considered to be part of the structure of any one atom in particular. In fact, the fact that electrons (and holes) can be induced by energy to move as part of the whole lattice structure is what enables the crystal lattice to function as a semiconductor in the first place. [2, 406.]

Diffusion coefficients, as the name suggests, are mathematical entities that represent the proneness of diffusion to happen in a semiconductor. The phenomenon of diffusion is the result of random thermal motion of particles, hence the dependence of the diffusion coefficients on temperature. In diffusion, particles migrate from areas of high concentration into areas of low concentration. [2, p.437-438, 478.]

4.1.3 Diffusion Lengths

Once the particle crosses over from the area of high particle concentration into the area of low particle concentration, it becomes a so-called minority carrier. In a semiconductor, the minority carriers are the electrons and the holes, and the minority carrier transport takes place over the so-called p-n junction. The p-n junction is formed near the depletion region due to the built-in voltage in a semiconductor (the concepts of the depletion region as well as the built-in voltage will be explained in the following subchapters). [2, p.417-418, 447.] The concept of the diffusion length is a physical representation of the average distance that a minority carrier can diffuse into a sea of majority carriers before being recombined [2, 450]. Recombination refers to an electron and a hole recombining, resulting in both the free electron and the free hole disappearing. There are various possible recombination mechanisms in a semiconductor (such as band-to-band recombination, trap-assisted recombination, Auger recombination, and surface recombination). [2, p.422, 425-426.] Mathematically, the diffusion length can be represented as the square root of the product of the

average minority carrier lifetime and the diffusion coefficient [2, 450]. Due to their dependence on the respective diffusion coefficients, the diffusion lengths are also temperature dependent [2, 478].

4.1.4 Built-in Voltage

An important technique in the manufacturing of semiconductors is one that is called doping. This refers to the introduction of impurities into the silicon crystal lattice, namely in the form of so-called donors and so-called acceptors. These impurities are bounded to the silicon atoms by covalent bonds; however, they contain a different number of valence electrons than silicon does. The most commonly used donor is phosphorus which has five valence electrons, whereas the most commonly used acceptor is boron which has three valence electrons. Since silicon has four valence electrons, and because these donors and acceptors are immobile within the silicon crystal lattice due to the covalent bonds, they create an electrostatic potential which is called built-in voltage. [2, p.417-418.]

As suggested above, the built-in voltage is temperature dependent, in fact, let us examine the equation for built-in voltage V_{bi} under thermal equilibrium:

$$V_{bi} = \frac{kT}{q} ln \left(\frac{N_D N_A}{n_i^2} \right) \tag{9}$$

Where k is Boltzmann's constant (8.617×10^{-5} eV/K), T is the temperature in Kelvin, q is the electron charge (1.6012×10^{-19} C or 1 eV), N_D is the number of donors per unit volume, N_A is the number of acceptors per unit volume, and n_i is the intrinsic carrier concentration at thermal equilibrium (more on which will follow shortly). [2, 420.]

4.1.5 Depletion Region Width

The concept of depletion region width is very strongly interlinked to the concept of built-in voltage. Basically, the depletion region is the part of the semiconductor where the electric field due to the built-in voltage is strong [2, 441]. Because the built-in voltage is temperature dependent, so is the depletion region width [2, 478].

4.1.6 Intrinsic Carrier Concentration

Of all the basic material properties of a semiconductor (i.e., in this case, a solar cell), the intrinsic carrier concentration is probably the most complicated one to explain. The mathematical equation for the intrinsic carrier concentration at thermal equilibrium n_i is as follows:

$$n_i = \sqrt{N_c N_v}\, e^{\left(\frac{-E_g}{2kT}\right)} \tag{10}$$

Where N_c is called the effective density of state of the conduction band and is defined as:

$$N_c = 2\left(\frac{2\pi m_n^* kT}{h^2}\right)^{\frac{3}{2}} \tag{11}$$

Whereas N_v is called the effective density of state of the valence band and is defined as

$$N_v = 2\left(\frac{2\pi m_p^* kT}{h^2}\right)^{\frac{3}{2}} \tag{12}$$

In equations 11 and 12, m_n^* and m_p^* are the effective masses of the electrons and the holes, respectively. As in equation 9, k is Boltzmann's constant (8.617×10^{-5} eV/K) and T is the temperature in Kelvin, whereas h is Planck's constant (6.626×10^{-34} Js). In equation 10 above, E_g is the band gap energy,

which has already been mentioned to be dependent on temperature. [2, 411-414.]

So, considering that temperature is a variable in all three equations above, 10, 11, and 12, the temperature dependence of the intrinsic carrier concentration is clearly shown. It is also worth bearing in mind that the equations 10, 11, and 12 are formulated at thermal equilibrium, yet they are still strongly dependent on the equilibrium temperature in question. The intrinsic carrier concentration at thermal equilibrium is an important material property in semiconductor analysis [2, 414].

The basic semiconductor physics explaining the dependence of solar cell performance on temperature is fundamental to understand. However, a more holistic mathematical model of a solar cell is required for practical software simulation.

4.2   Impedance Matching

In order to properly understand practical solar cell applications, one must have a good understanding of the environmental conditions in which solar cells will be used. While work in the laboratory is necessary to develop more efficient solar cells, the reality remains that most solar cells on the market today are relatively inefficient units that are popular primarily due to their affordability compared to more advanced models.

It has been established that the efficiency of a solar cell depends primarily on two different environmental factors: temperature and irradiance. Since solar cells may be applied in environmental conditions where both of these vary significantly, replicating real world applications under laboratory conditions provides a challenge.

Due to the varying efficiency of the solar cell under changing environmental conditions, some sort of a system that facilitates the electrical implementation of the solar cell to adapt to changes in the environment is needed. In order to properly understand the requirements for such a system, we must look into some realities of practical applications of small-scale power production systems.

Firstly, we must understand that the electrical output of a solar cell is dependent upon temperature and irradiance. Secondly, we must keep in mind that we will be dealing with a system of various interconnected solar cells with it most probably being a mixture of series and parallel connections. Thirdly, we have to understand the basics of power delivery from source to load in such a system. The maximum efficiency of power delivery in a system where the source and load are connected in series occurs when the load resistance is made as great as possible. This is simply because the overall resistance of the source and the load combined determines the current in the system, and the power delivered to the load will be proportional to the voltage drop in the load compared to the voltage drop at the source. However, this can be problematic because the output power of a solar cell is quite low, which means that if the current is considerably limited by a high load resistance, the absolute output power may be negligibly small despite the seemingly high efficiency. The maximum power delivered to a load is achieved when the load resistance matches the source resistance, however, in this case half of the produced power output of the source is lost in the source itself so that the overall efficiency is not very high. [1, 88-89.]

An established circuit that provides impedance matching between the source and the load is a pulse width modulation (PWM) controlled direct current to direct current voltage converter, namely a boost converter or a buck converter. The pulse width modulation inherent to these systems can be made to respond to changes in the electrical and the environmental conditions by means of a microcontroller. This enables procedures such as maximum power point tracking (MPPT), which helps to find the optimal electrical conditions so that the

most power can be drawn from the solar cell arrangement. There are various different procedures by which MPPT can operate, some of which will be investigated in this study.

Consider, for example, a boost converter which utilizes PWM in order to regulate an output voltage which will be higher than the voltage at the input of the converter. Such a device will be convenient in addition to a solar panel if the required load voltage is higher than that of the solar panel's output. The alternative would be to connect various solar panels in series in order to achieve a higher output voltage. However, this would pose problems since the output voltages of solar panels are not regulated in the way that a boost converter's output voltage will be. In the case that a higher output current, but lower voltage, is needed, as is often the case for efficient battery charging, for example, a buck converter ought to be placed in the system instead of a boost converter. [3, 169.]
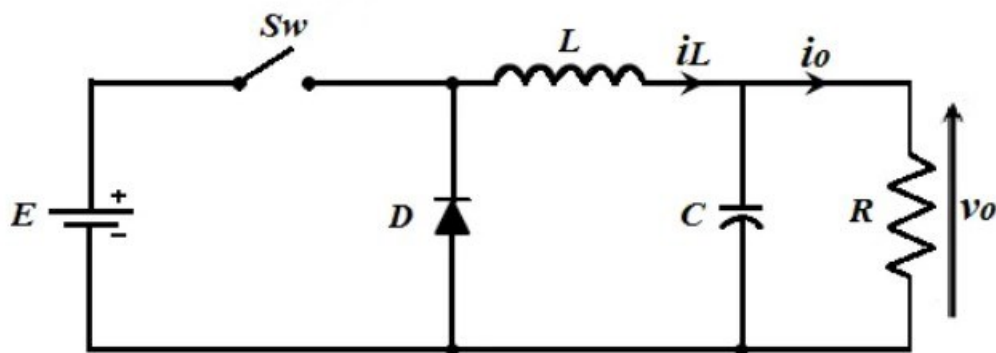

Figure 19. A simplified schematic of a buck converter [11].

Figure19 above represents a considerably simplified schematic of a direct current to direct current buck converter. In figure 19, the amount of time that the switch Sw is closed in proportion to the time that the switch Sw is open is determined by an external PWM controller (not shown). In a real circuit, the switch S1 would be implemented with either a metal oxide semiconductor field

effect transistor (MOSFET) or an insulated gate bipolar transistor (IGBT). [3, 175; 11; 12, 480; 13.]

Consider still the circuit presented in figure 19. The output inductor L will be opposing changes in the current through itself. The counterelectromotive force induced will depend on the rapidity of the change in current. The external PWM controller is capable of opening and closing the switch Sw at an elevated pace. When the switch Sw is closed, the inductor L is connected to the positive output polarity of the voltage source E, and when the switch is open, the inductor is connected to approximately minus 0.7 volts (due to the forward voltage drop of the diode D). For these reasons, the current through the inductor L (designated *i(L)* in figure 19) will vary somewhat smoothly between a maximum value and a minimum value. The average between these two values will constitute the output current (designated *i(o)* in figure 19) into the load (designated *R* in figure 19). [12, 480.]

In figure 19, imperfections in the switch Sw and the diode D may cause a considerable source of electromagnetic interference [12, 480]. However, these types of buck converter circuits, as well as corresponding boost converter circuits, have become commonplace in many applications, including solar power. Another issue, stemming directly from the real-world electrical properties of the output inductor (L in figure 19), is the generation of ripple in the output voltage during the operation of the converter circuit [12, 480]. Such ripple in the voltage output of the circuit can be alleviated by the use of additional circuitry, such as a snubber circuit [13].
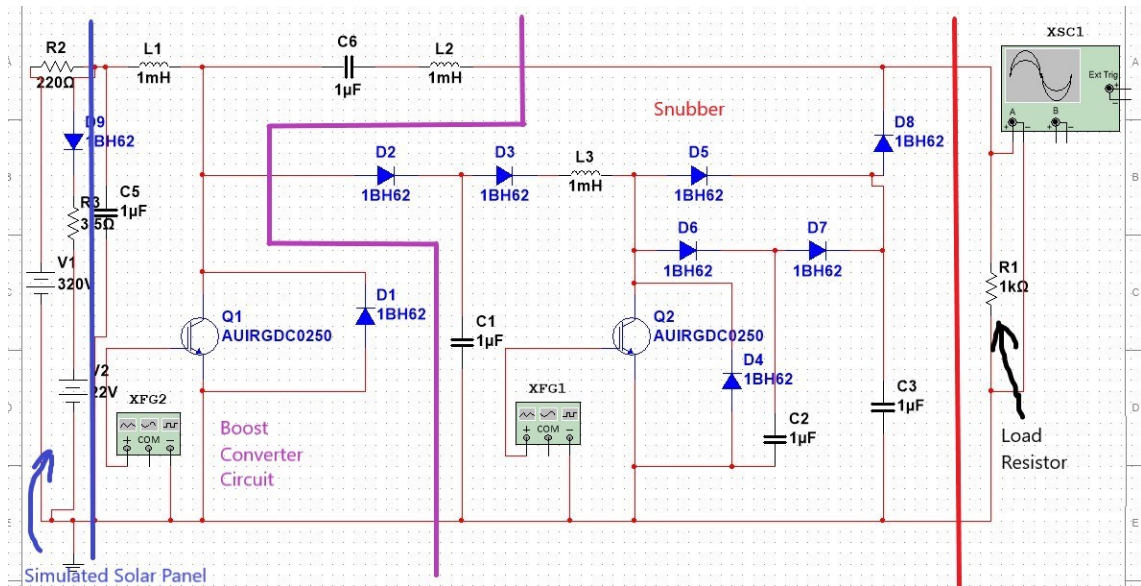
Figure 20. A simulated boost converter featuring a snubber circuit. The converter has its input fed from a simulated solar panel output. This simulation is made using the National Instruments MultiSim software.

Figure 20 represents the simulation of a much more sophisticated circuit for a solar cell application, this time utilizing a boost converter and a snubber circuit. In figure 20, the direct current voltage supplies V1 and V2 as well as the resistors R2 and R3 and the diode D9 are providing a virtual simulation of a real-world solar panel output [10]. The actual boost converter circuit consists of the input filter capacitor C5, the connecting capacitor C6, inductors L1 and L2 on the primary and secondary sides, respectively, of the boost converter and the switching elements provided by the function generator XFG2, the IGBT Q1 and the diode D1. R1 is used as the load resistor and the oscilloscope XSC1 is used to measure the output current and output power. The remaining electrical components in figure 20 comprise the snubber circuit with the purpose to reduce the output voltage ripple. [13.]

The values of the electrical components in figure 20 have been completely arbitrarily chosen, without practically any consideration for how the circuit would operate in practice. Even with these values, the operation of the circuit in figure 20 was determined via simulation to be properly functioning as a boost converter if the load resistance was at least 50 Ω. This seems like a reasonable condition for operation in real-world environments.

All in all, the use of PWM controlled direct current to direct current voltage converters is already globally established among small-power solar panel applications. Refinements in this application, particularly ones that maintain the affordability of the system, are an extremely promising area of study. As already suggested, these refinements usually involve control of the operating conditions of the direct current to direct current voltage converter. The focus of this study is now shifted into investigating some of these refinements.

4.3 Maximum Power Point Tracking (MPPT)

Further refinements into the operation of a direct current to direct current voltage converter can be achieved using algorithms such as maximum power point tracking (MPPT). These algorithms can be programmed into the microchip in the converter itself. It is also possible to utilize such algorithms by means of an external programmable device.

In any case, it is first necessary to define the maximum power point of a solar panel system's operation. It is generally assumed that there exists only one maximum power point so that the change in power in relation to whatever parameter is being manipulated will be zero at the maximum power point. This should be clear based on the well-known laws of differential calculus. A common method implemented in a real-world controller is known as the perturb and observe (P&O) method [14]. In this method, the output voltage of a converter is constantly being altered in small steps, and the resulting change in output power is measured. As long as the measured output power keeps increasing, the changes in the voltage of the controller are being made to the same direction (i.e., increasing or decreasing output voltage of the controller). Once the measured output power decreases when the voltage is altered, the gradual changes in voltage change their direction and remain in the new direction until the measured output power decreases again. Because this

process is maintained constantly, the perturb and observe algorithm makes it possible to draw a maximized power yield from the solar panel system despite changing environmental conditions, such as temperature and irradiance. [3, 179.]

Exact details of a perturb and observe algorithm, or any other MPPT algorithm, will depend on the details of the type of controller applied. Figure 21 shows an example of a buck converter used with a perturb and observe algorithm that is applied using the LabVIEW graphical programming language [14]. Figure 21 features programmed equations that will be used to determine the optimal duty cycle of the buck converter's operation to achieve operation at the maximum power point.
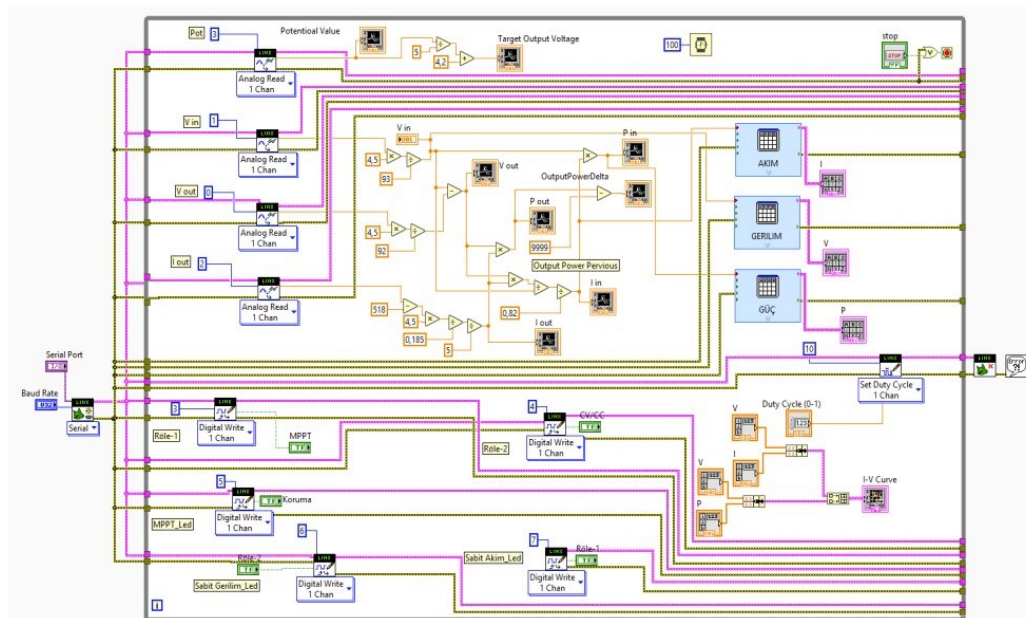

Figure 21. Example block diagram of a LabVIEW program utilizing the P&O MPPT algorithm. The controlled parameter is the PWM duty cycle of a buck converter. [14.]

MPPT is known to be an established technique with good applicability. However, potential improvements as well as novel approaches to the MPPT algorithm have been suggested. One particular approach, namely that of incremental conductance MPPT, will be explored in what follows.

5   Incremental Conductance Method

Another MPPT algorithm often used in solar power applications is the incremental conductance algorithm [15]. It is also based on the reality that the derivative of the power at the maximum power point relative to voltage (or any other variable) is zero. Mathematically this is presented as

$$\frac{dP}{dV} = 0 \tag{13}$$

Where *P* denotes power and *V* denotes voltage. The mathematical idea behind the incremental conductance MPPT algorithm is illustrated in figure 22, which shows the conditions at the maximum power point as well as on the left side and on the right side of the maximum power point when the output power is plotted as a function of the output voltage. Note, however, that figure 22 assumes a simple relationship between these two measures, with a single maximum power point that can be seen clearly from the graph.
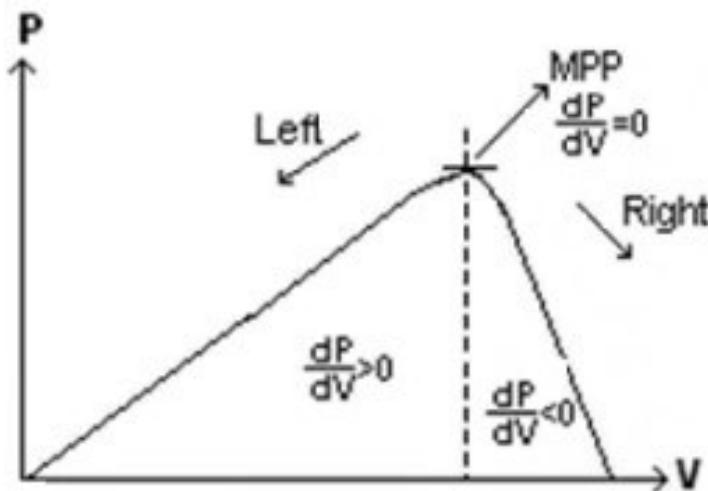

Figure 22. Illustration of the determination of the maximum power point [15].

On the other hand, according to the basic laws of electrical circuits, power is the product of current *I* and voltage *V*:

$$P = IV \tag{14}$$

Now consider the variation of the output current of a direct current to direct current voltage converter as a function of the output voltage of the converter, *I(V)*. In this way, equation 14 can be presented as:

$$P = I(V)V \tag{15}$$

I(V) in equation 15 simply means that the current *I* is represented as a function of the voltage *V*. The product *I(V)V* is the product of this current with that same voltage whose function it is represented as. Taking into consideration the rule for the derivative of the product of two functions, the derivative of equation 15 becomes:

$$\frac{dP}{dV} = V\frac{dI(V)}{dV} + I(V) \tag{16}$$

At the maximum power point, equation 13 holds so that this means that:

$$\frac{dI(V)}{dV} = -\frac{I(V)}{V} \tag{17}$$

This formulation of the fundamental equation of incremental conductance MPPT, describing the condition at the maximum power point, is illustrated in figure 23 below. Basically, figure 23 is the same as figure 22, only the mathematical formulations on the left side of the maximum power point, at the maximum power point, and on the right side of the maximum power point are different (but equal to the ones presented in figure 22).
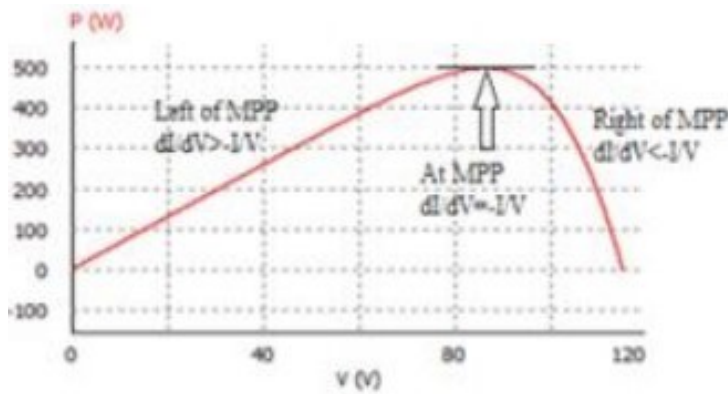
Figure 23. Another approach to the determination of the maximum power point, compare with figure 22 [16].

If a controller can be programmed to minimize the difference between the derivative of the current as the function of the voltage, and the inverse value of the measured current divided by the measured voltage, it is successfully implementing the incremental conductance algorithm and should make operation at the maximum power point possible. [15.]

Programming languages should not be expected to be able to calculate derivatives, though. This means that an acceptable approximation for the derivative of the current as the function of the voltage is needed. A rudimentary approximation, although one that should be accurate enough for low-cost applications, can be formulated by means of a recent measured value of the output current, to be designated in the following as $I_1(V_1)$ and assuming a basic relationship between the current and the voltage. This gives:

$$\frac{dI(V)}{dV} \approx \frac{I_2(V_2) - I_1(V_1)}{V_2 - V_1} \tag{18}$$

Equation 18 above is based on the definition of the derivative and is easily implemented in a computer programming algorithm. $I_2(V_2)$ is the new value of the output current that is measured at the instant that the output voltage has the value V_2. According to the definition of the derivative, equation 18 provides an approximation to it as the change in the value of the measured output current divided by the change in the value of the measured output voltage. This is

possible because the output current was assumed to be a function of the output voltage and hence presented as such.

The incremental conductance algorithm, based on the equations above, can be presented as a flow chart as in figure 24 [16].
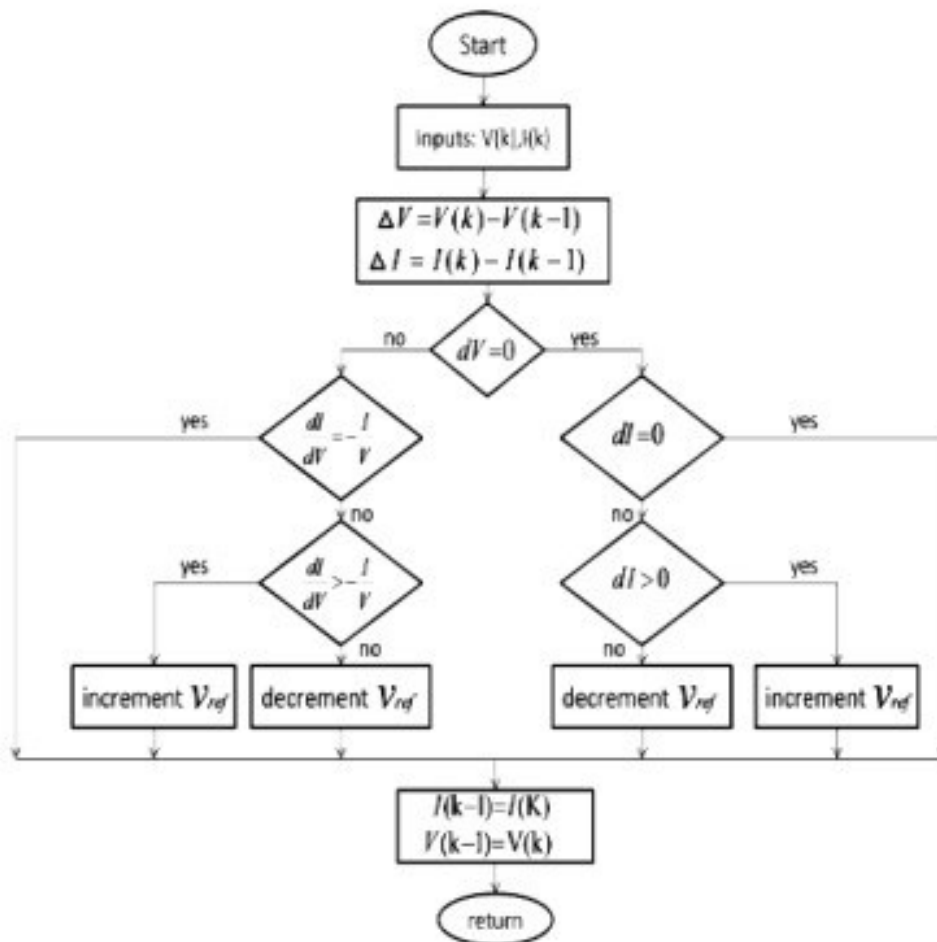

Figure 24. The incremental conductance MPPT algorithm presented as a flow chart [16].

In figure 24, V_{ref} refers to the output voltage of a direct current to direct current voltage converter that is used in the incremental conductance MPPT system. In a simple system, this reference voltage is the same as the output voltage of the direct current to direct current converter that is connected to a load. Also in a

simple system, the change in the reference voltage can be assumed to be implemented by altering the duty cycle of the direct current to direct current converter by means of pulse width modulation (PWM) [3, 178-179; 14].

The flow chart in figure 24 requires additional attention. Note that the first condition established in the flow chart is whether dV equals zero or not. This is done in order to avoid dividing by zero in the computer program, since the change in the measured output voltage appears in the denominator on the left-hand side of the mathematical expression in equation 17. This corresponds to the difference between two successive measured values of the output voltage in the denominator in the mathematical expression on the right-hand side of equation 18. Should there be no change in the value of the measured output voltage, the flow chart then instructs the program to not change the reference voltage, or increase the reference voltage, or decrease the reference voltage, depending on the value of the measured output current.

There have been reports of incremental conductance based MPPT algorithms devised with the LabVIEW graphical programming language presented earlier [16; 17]. However, these results do not involve a real-time MPPT device, nor is the exact type of direct current to direct current voltage converter that is utilized ever specified in these studies. Their results have to be considered preliminary, although encouraging. In one study, a LabVIEW-based simulation model provided results that were well in agreement with measured results as well as calculations based on parameters provided by the solar panel manufacturer in the data sheet [17]. In another study, a simulation was made that was efficient in tracking a local maximum power point but could not track a global maximum power point in the presence of a more complicated relationship between converter output voltage and achieved power output. This type of a more complicated relationship may occur due to shifts in environmental conditions, such as varying irradiance. [16.] The inability of the algorithm to track a global maximum power point in circumstances like these is the direct result of the algorithm utilizing a simple mathematical model involving only one value where the derivative of the power output in relation to the output voltage is zero, i.e.,

the maximum power point. Pictures of the different implementations of incremental conductance MPPT in solar power applications in LabVIEW are provided in figures 25–33.

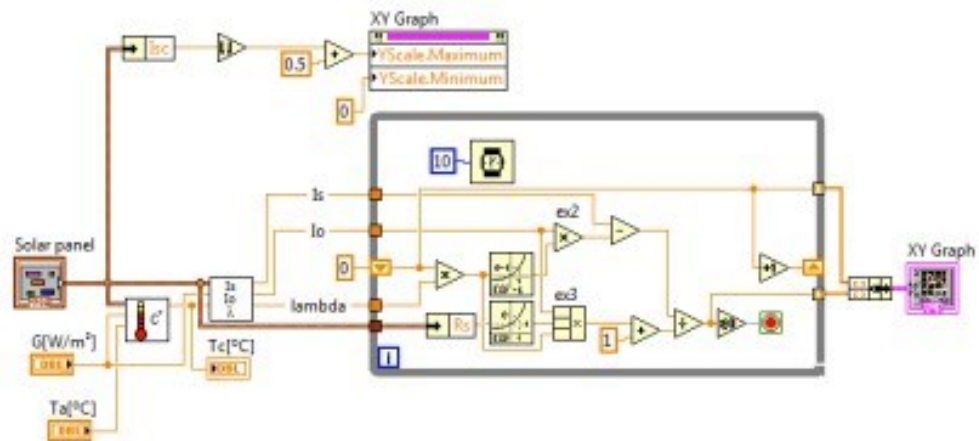One type of a LabVIEW model of a solar panel is presented in figure 25 below.

Figure 25. Example block diagram of a LabVIEW application modelling a solar panel [17].

The practical incremental conductance MPPT application of the solar panel model presented in figure 25 is shown in figure 26 below.
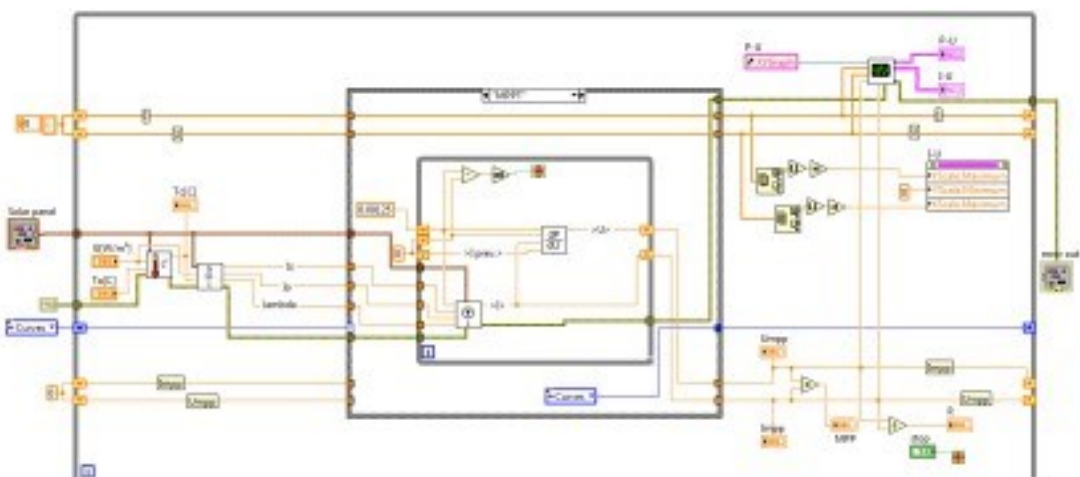

Figure 26. Example block diagram of a LabVIEW application utilizing the incremental conductance MPPT algorithm for the output of a solar panel [17].

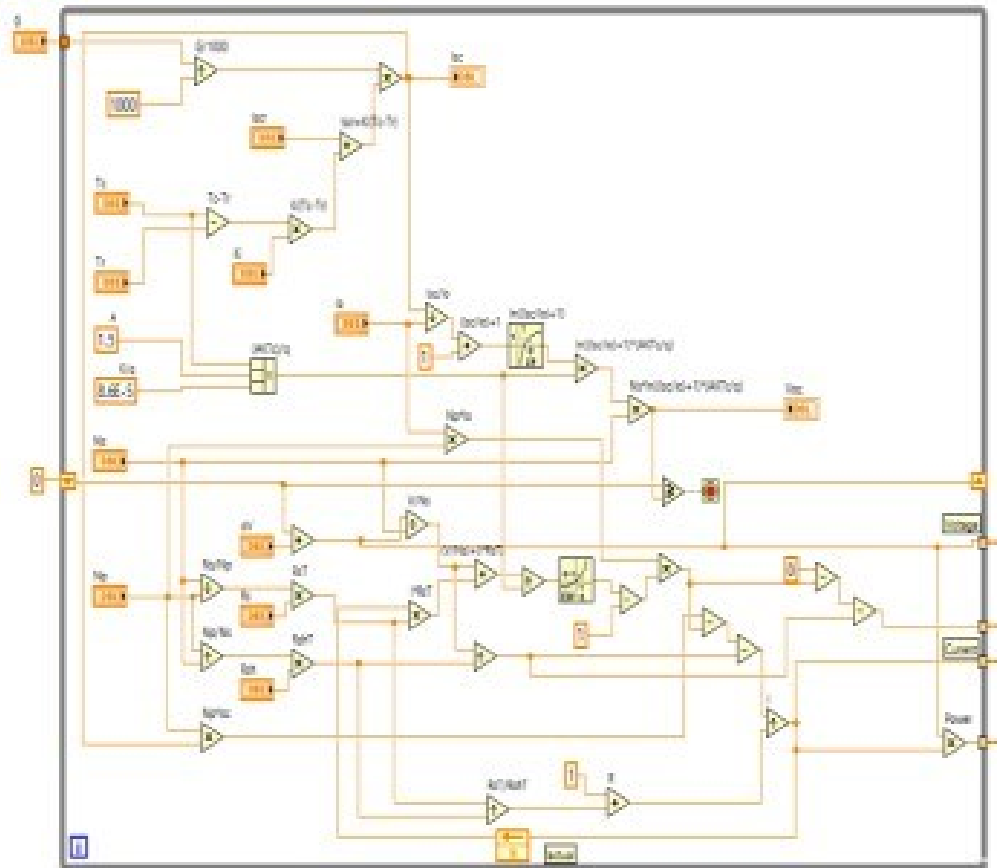Another type of a solar panel LabVIEW model can be seen in figure 27.

Figure 27. Example block diagram of another LabVIEW application simulating a solar panel [16].

Figure 28 presents the LabVIEW application of the incremental conductance MPPT algorithm when there has been no measured change in the output voltage and no measured change in the measured output current either. Figure 28 also shows the corresponding branch of the flow chart presenting the incremental conductance MPPT algorithm next to the LabVIEW block diagram. The solar panel model utilized in the application presented in figures 28–33 is the one shown in figure 27.

Consider the detail of the LabVIEW block diagram presented in figure 28. Three input connections can be seen entering from the left. One of these is labelled *V(K)-V(K-1)*, another one is labelled *I(K)-I(K-1)*, and the third one is unlabelled in the figure (although it will be found out to represent the reference voltage, i.e., V_{ref} in the flow chart of figure 24). The input labelled *V(K)-V(K-1)* represents the

difference between the latest measured value of the output current, namely *V(K)*, and the previous measured value of the output current, namely *V(K-1)*. The result of this subtraction is connected to the equals zero comparison function. The comparison function accepts a numeric input and produces a Boolean output, meaning a true/false value at the output. The equals zero comparison function simply means that the Boolean value at the output is set to be true if the numeric input to the comparison function equals zero. In the case that the numeric input value to the equals zero comparison function does not equal zero, the Boolean value at the output of the equals zero comparison function is set to be false. Since the input to this equals zero comparison function is *V(K)-V(K-1)*, the output of this equals zero comparison function will be true if and only if *V(K)-V(K-1)* equals zero, i.e., if *V(K)* and *V(K-1)* are the same value, which means that there is no change in the two latest values of the measured output voltage.

The Boolean value at the output of this equals zero comparison function is then connected to the outmost case structure. Because in the case presented in figure 28 there is no change in the measured output voltage of the system, the option *true* can be seen active at the top of the grey rectangle representing this case structure. Everything that takes place inside the outermost grey square in figure 28 is part of this case structure. After it has been determined that there is no change in the measured output voltage, the next step is to determine whether there has been change or not in the measured output current. This is achieved with another equals zero comparison function, this time connected to the input labelled *I(K)-I(K-1)*, because that input represents the difference in the two latest measured values of the output current. The *I(K)-I(K-1)* input can be seen directly connected through the outermost case structure, because its value has no effect on the determination of the change in the measured output voltage. It is only inside the outermost case structure where the *I(K)-I(K-1)* input can be seen connected to its respective equals zero comparison function. The Boolean output of this new equals zero comparison function is then connected to its own case structure, which is located inside the outermost case structure in figure 28. In the case presented in figure 28, the output current is also

determined to have remained unchanged. For this reason, the operation of the circuit is considered to already be at the maximum power point, and no further actions are taken by the LabVIEW program until either the value of *V(K)-V(K-1)* or the value of *I(K)-I(K-1)* moves away from being zero.

The third unlabelled input entering from the left side of the detail of the LabVIEW block diagram in figure 28 is now considered. This input proceeds unmanipulated through both case structures in the part of the block diagram that is shown. This is the input corresponding to the value of V_{ref} in the incremental conductance MPPT flow chart presented in figure 24. In the situation that there is no measured change in the output current in addition to there being no measured change in the output voltage, the system is considered to already be operating at the maximum power point so that the reference voltage is not manipulated by the program. This concludes the explanation of the part of the LabVIEW block diagram shown in figure 28 below.
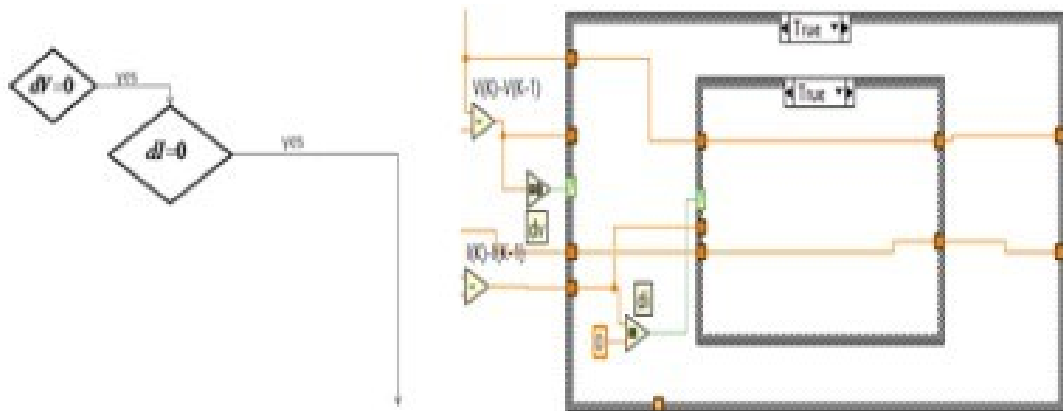

Figure 28. Block diagram of a LabVIEW program corresponding to the branch of the incremental conductance MPPT flow chart where there is no change in the measured output voltage and no change in the measured output current either. This results in the reference voltage staying the same. [16.]

Another scenario, namely one where there has been no change in the measured output voltage, but the measured output current has decreased, is presented in figure 29 below.

In figure 29, the same three inputs as in figure 28 can be seen entering from the left side of the depicted part of the LabVIEW block diagram. These three inputs are the *V(K)-V(K-1)* input, the *I(K)-I(K-1)* input, and the third unlabelled input, the value of which corresponds to the value of the reference voltage V_{ref}. In the case depicted in figure 29, the *I(K)-I(K-1)* input has a nonzero value, so that the option *false* is activated in the case structure which is connected to the Boolean output of the equals zero comparison function which has the difference *I(K)-I(K-1)* as its input. Inside this second case structure in figure 29, the *I(K)-I(K-1)* input can then be seen connected to another comparison function, namely the greater than comparison function, which has had the value zero assigned as the constant value that the other input value is being compared to. In this case that other input value is the value of the *I(K)-I(K-1)* input since that input is connected to this greater than comparison function. The Boolean output of the greater than comparison function is the connected to a third case structure. This third and innermost case structure in figure 29 also has two options, namely *true* and *false*, of which only one can be active at a time. Because in the case depicted in figure 29 the measured output current value has decreased from the previous measured output current value, the option *false* can be seen activated on the top of the innermost case structure in figure 29. In the incremental conductance MPPT algorithm this is interpreted as a command to decrease the reference voltage V_{ref}. A numeric function can be seen used to subtract a constant value of 0.00125 from the (illustrative) wire that carries the value of the reference voltage inside the innermost case structure in figure 29. This represents the step of decreasing the value of the reference voltage. The new value of the reference voltage, which has been lowered by this constant value of 0.00125, will be assigned as the new value of the V_{ref} output variable.
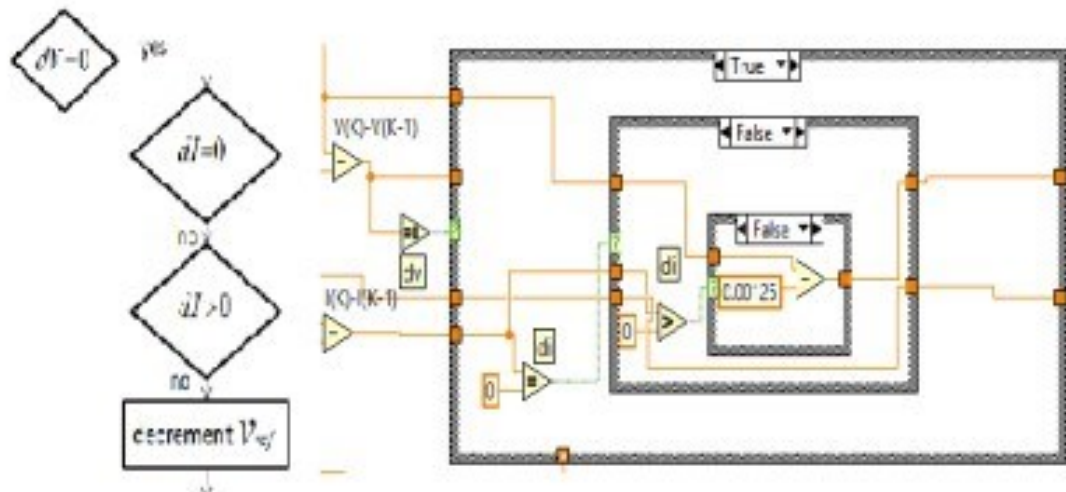
Figure 29. Block diagram of a LabVIEW program corresponding to the branch of the incremental conductance MPPT flow chart where there is no change in the measured output voltage, but the measured output current has decreased. This results in a decrease in the reference voltage. [16.]

On the other hand, figure 30 shows how the program operates if there has been an increase in the measured output current in the absence of a change in the measured output voltage.

As in figure 29, a total of three case structures can also be seen in figure 30. Once again, these are all connected to the Boolean outputs of comparison functions in the LabVIEW code. The outermost case structure determines its selected case from the Boolean output of a equals zero comparison function that is connected to the *V(K)-V(K-1)* input (the Boolean output of this equals zero comparison function is *true* in the case of figure 30). The second and third case structures determine their selected cases from the Boolean outputs of two different comparison functions that are both connected to the *I(K)-I(K-1)* input. The middle case structure has its case selected based on whether there has been a change in the measured output current (the case selected in figure 30 is *false*) and the innermost case structure has its case selected based on whether the measured change in the output current is greater than zero (the case selected in figure 30 is *true*). Correspondingly to this part of the incremental conductance MPPT flow chart, the reference voltage is increased in the constant step of 0.00125.
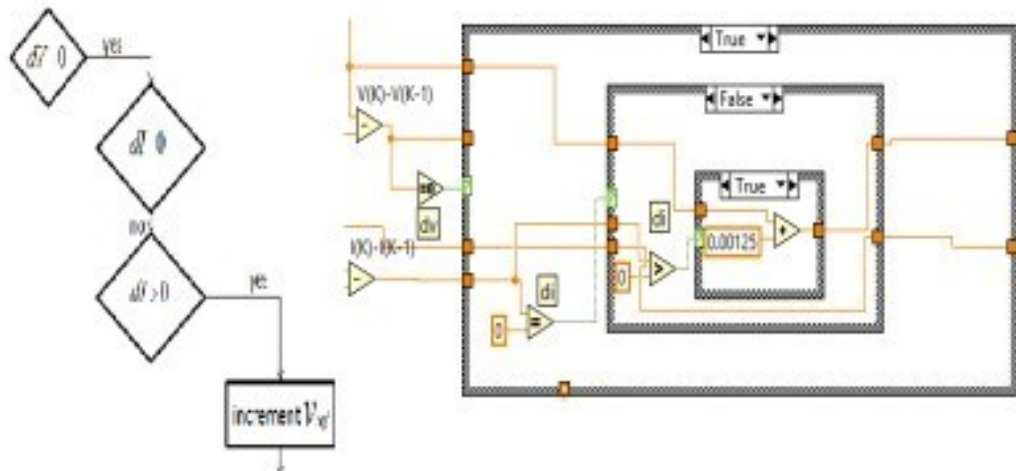
Figure 30. Block diagram of a LabVIEW program corresponding to the branch of the incremental conductance MPPT flow chart where there is no change in the measured output voltage, but the measured output current has increased. This results in an increase in the reference voltage. [16.]

The possibility that the measured output voltage has changed is presented in figures 31–33 below. Figure 31 shows one scenario where the measured output has changed, along with the corresponding adjustment of the reference voltage and the corresponding branch of the incremental conductance MPPT flow chart.

The use of case structures and comparison functions in figures 31–33 is like what was examined in figures 28–30 above. Additional numeric functions can be seen inside the case structures of figures 31–33. These numeric functions are used to carry out the divisions and other necessary calculations to determine the corresponding branch of the incremental conductance MPPT flow chart.
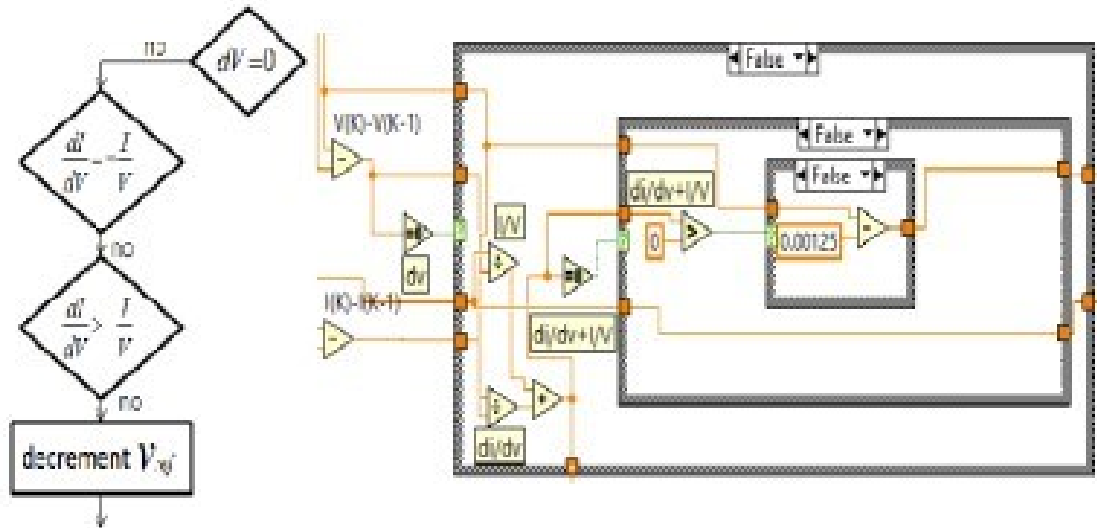
Figure 31. Block diagram of a LabVIEW program and the corresponding branch of the incremental conductance MPPT flow chart. In this case there has been change in the measured output voltage, and the appropriate adjustment of the reference voltage is carried out. [16.]

Figure 32 shows another scenario where the measured output voltage has changed.
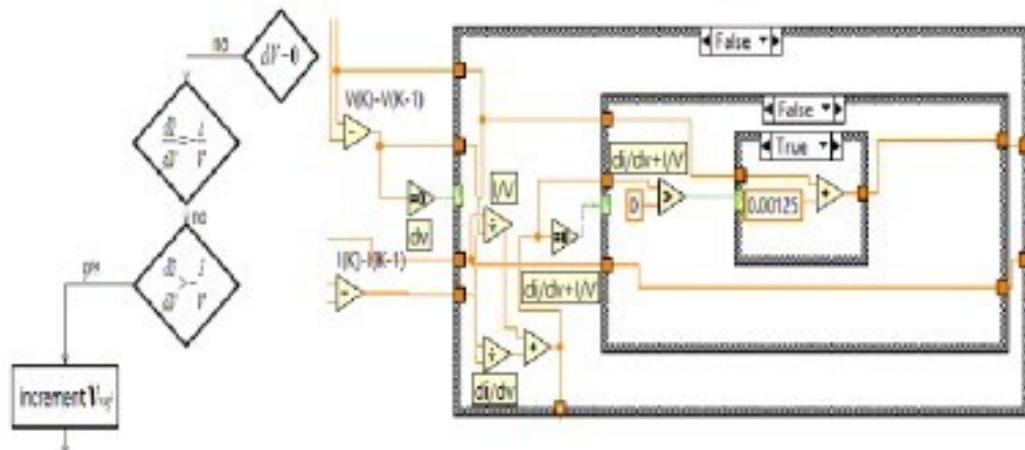

Figure 32. Block diagram of a LabVIEW program corresponding to another branch of the incremental conductance MPPT flow chart where there has been change in the measured output voltage [16].

And finally, figure 33 represents the scenario where the system is determined to be operating at the maximum power point despite a measured change in the

output voltage. Figure 33 concludes the present investigation of this particular LabVIEW application.
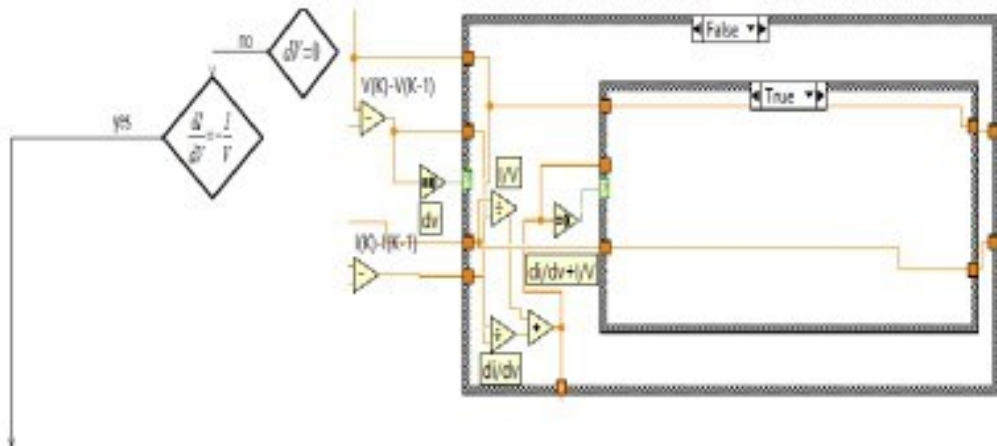

Figure 33. Block diagram of a LabVIEW program corresponding to the branch of the incremental conductance MPPT algorithm where the system is determined to be operating at the maximum power point. The reference voltage is retained at its present level. [16.]

As stated above, a considerable limitation of the LabVIEW programs investigated this far is the lack of real-time measurement and control capabilities. The remaining work in this study will attempt to address this limitation and overcome it.

6   Real-Time Measurement and Control Program

At this point, the need for a computer program that can measure the output voltage and the output current of a direct current to direct current voltage converter, as well as being one that can control the duty cycle of the PWM algorithm of that same direct current to direct current voltage converter, has been established. An additional need is that for such a program that would also be capable of the measurements and PWM duty cycle control in a real-time

application. There have been examples of programs in the LabVIEW graphical programming language that have been capable of doing these things, but only in a purely simulated environment, not while attached to real-world measuring devices that operate with analogue voltage and current signals. National Instruments, the manufacturer of LabVIEW, provides the NI-DAQmx system as an interface for such real-time real-world measurement and control applications.

To devise a LabVIEW program that uses the NI-DAQmx interface in a real-time real-world incremental conductance MPPT application, an understanding is needed of what exactly is being measured and, more importantly, what exactly is being controlled. As a preliminary example, the Analog Devices LTC6992 PWM control circuit is considered. The data sheet of the LTC6992 [18] expresses that the PWM duty cycle is determined by a voltage input in the MOD pin of the device. The duty cycle basically follows that modulation signal level in volts, so that a 10% duty cycle is achieved by a modulation signal level of 0.1 V and a duty cycle of 90% is achieved by a modulation signal level of 0.9 V. These are the minimum and maximum values of the duty cycle to be implemented in the real-time LabVIEW application that is being devised. Figure 34 shows the PWM control circuit that was designed for this application with the online tool provided by the manufacturer [19]. The output frequency is 30 Hz.
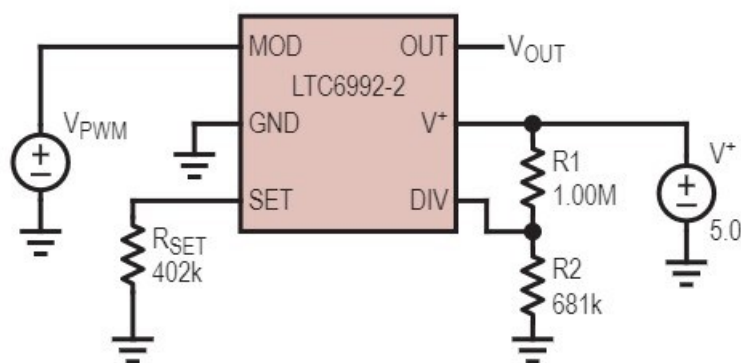

Figure 34. LTC6992 circuit suitable for this application designed with the TimerBlox LTC6992: PWM Web-Based Design Tool [19].

This type of an application requires a LabVIEW program where an output voltage depending on measured voltage and current is calculated. The voltage and current values are the voltage and current at the output of the direct current to direct current voltage converter. The determination of the maximum power point will happen according to the model presented in equations 17 and 18. This model is also presented in the flow chart of figure 24.

An actual circuit that utilizes the LTC6992 and that could be used to implement this type of incremental conductance MPPT control in relation to a boost converter is presented in figure 35 below. The IRLZ44N MOSFET was chosen because of its compliance with the LTC6992 by making it possible to turn the MOSFET on and off by applying the PWM output voltage of 3.3 V to the gate of the MOSFET as in the circuit presented in figure 35. The PWM control circuit part of the application in figure 35 was designed with the TimerBlox LTC6992: PWM web-based design tool provided by the manufacturer of the LTC6992 [19]. The simulated solar panel in figure 35 is the same one as in figures 17 and 20 [10].
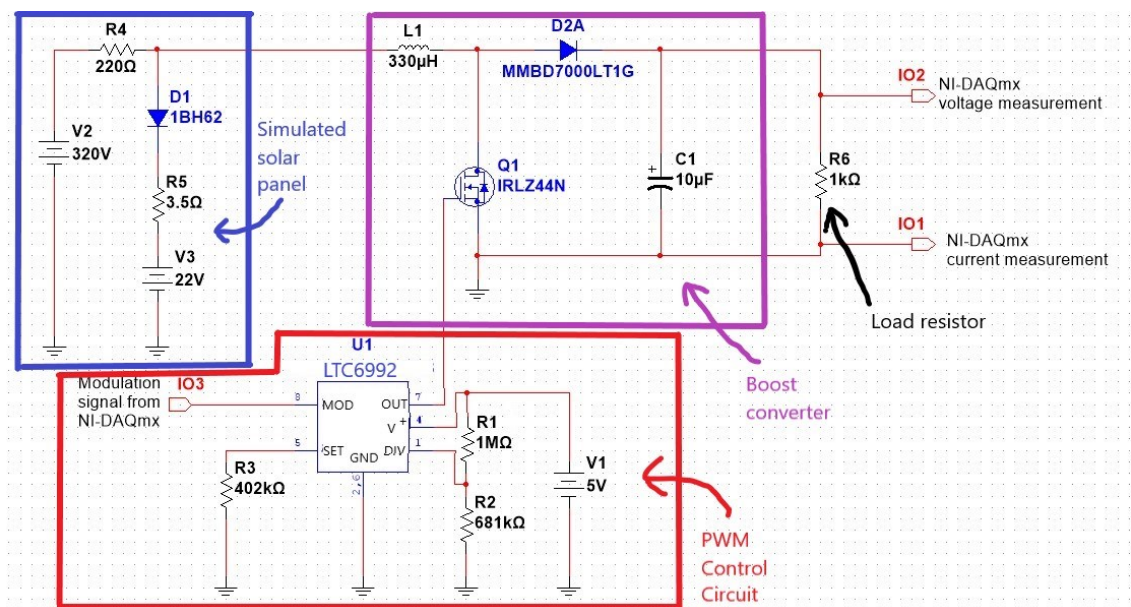

Figure 35. Circuit schematic of the proposed real-time measurement and incremental conductance MPPT application. Note the slightly different pin configuration of the LTC6992 from figure 34.

The relationship between the control signal, which is a voltage level provided as an analogue output of the LabVIEW program, the ramp voltage (also referred to as the carrier signal), and the output pulse width is presented in figure 36. The wider output pulse width will result in a higher average voltage at the output of the direct current to direct current voltage converter. Due to the circuitry utilized in the direct current to direct current voltage converter, this higher average voltage level will be smoothed (or, namely, averaged) into a higher constant output voltage level. [20.]
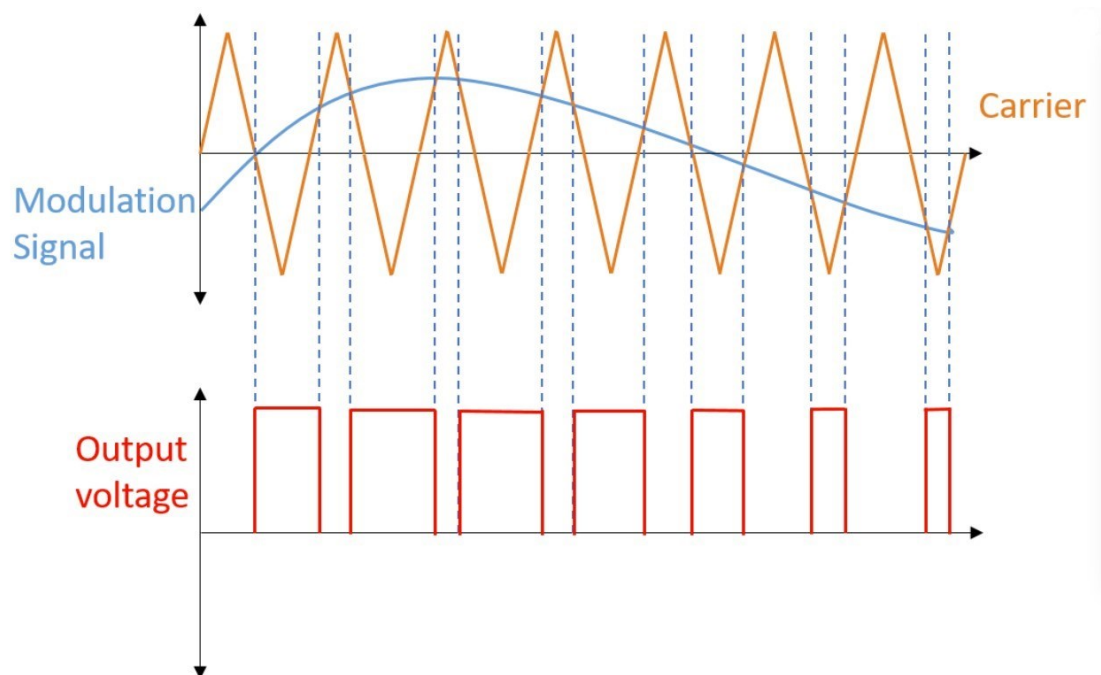

Figure 36. Diagram of the PWM principle of operation. A higher modulation signal level results in a wider output pulse width. [20.]

Ultimately, the devised real-time LabVIEW program is presented in figures 37–42. The utilization of 100 milliseconds between samples of the output voltage and current of the direct current to direct current voltage converter as well as the increments and decrements of the pulse width modulation signal voltage in steps of 1.25 millivolts are taken from LabVIEW programs presented earlier. Also, in a manner similar to the LabVIEW program presented in figures 27–33, the different possibilities expressed in the flow chart of figure 24 are programmed by using the case structures in LabVIEW. Furthermore, the use of

shift registers in order to store the previous values of the measured output voltage and current as well as the previous value of the pulse width modulation signal voltage is common to both LabVIEW programs. Shift registers can be seen connected to the while loop, which is the outermost grey rectangle in figures 37 and 38. A difference can be noted in that the possibility of the change in the output voltage being zero is programmed in the earlier LabVIEW program by using the equals zero comparison function, whereas in this real-time program that is presently being devised, it is programmed using the does not equal zero comparison function. The option *false* in the outermost case structure of the earlier program corresponds to the option *true* in the outermost case structure of the new program, and vice versa. Also, the LabVIEW application presented in figures 37–42 includes NI-DAQmx related functions (such as create channel, start, read, write, stop, and clear) that are missing from the applications presented earlier. Apart from the read and write ones, these are located outside the while loop (as can be seen in figures 37 and 38). The NI-DAQmx related task wiring (purple) and error wiring (yellow/black) can be seen in figures 37–42.

The NI-DAQmx physical channels in this new program are channel number one (designated "DAQmx Physical Channel" in figures 37 and 38) for the measured output current, channel two for the measured output voltage, and channel three for the pulse width modulation signal, which is assigned as an analogue output voltage.

Figure 37 illustrates the operation of the new LabVIEW program when neither the measured output voltage nor the measured output current have changed. The operation is determined to be at the maximum power point.
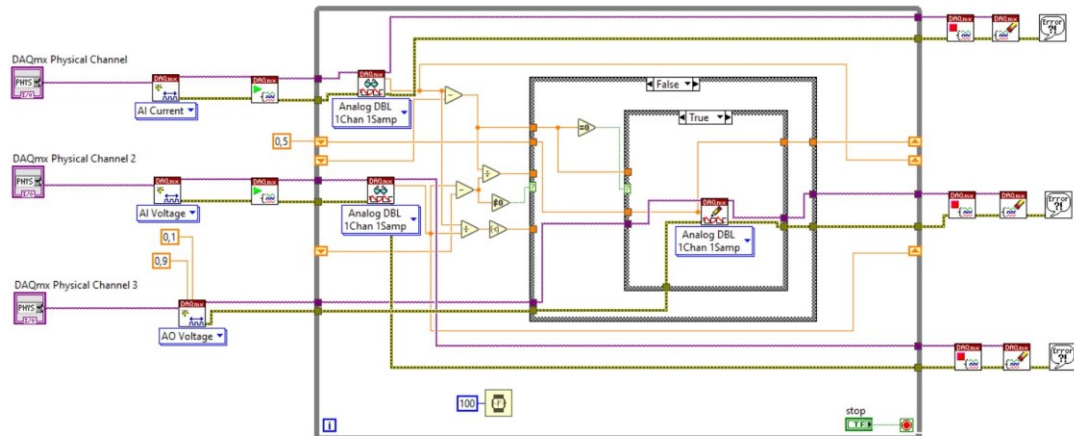
Figure 37. Block diagram of the devised real-time LabVIEW program. The depicted operation corresponds to that of figure 28.

Figure 38 illustrates the operation of the devised real-time LabVIEW program as the measured output voltage has not changed, but the measured output current has decreased.
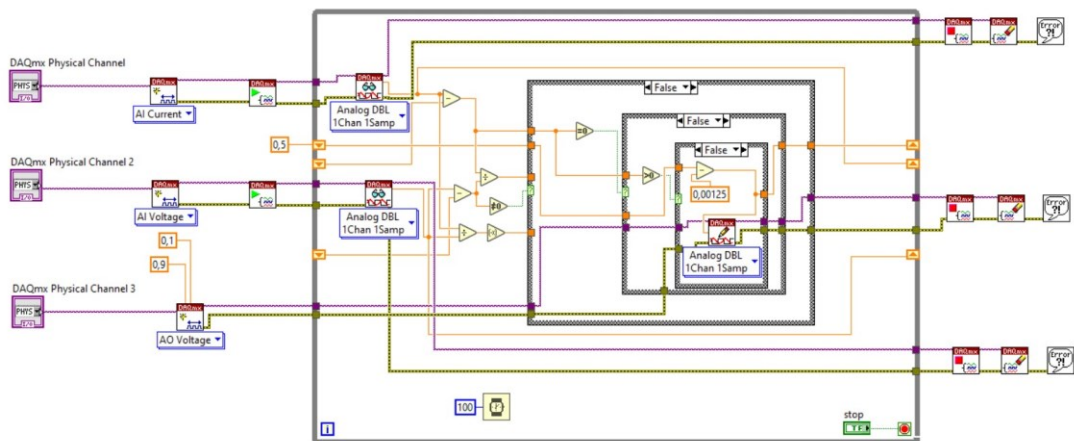

Figure 38. Block diagram of the devised real-time LabVIEW program. The depicted operation corresponds to that of figure 29.

Figure 39 illustrates the operation of the real-time LabVIEW program as the measured output voltage has remained the same, but the measured output current has increased. From figure 39 onwards, pictures of this new LabVIEW

program will focus on the case structures part of the block diagram, namely the part that actually is different in each image.
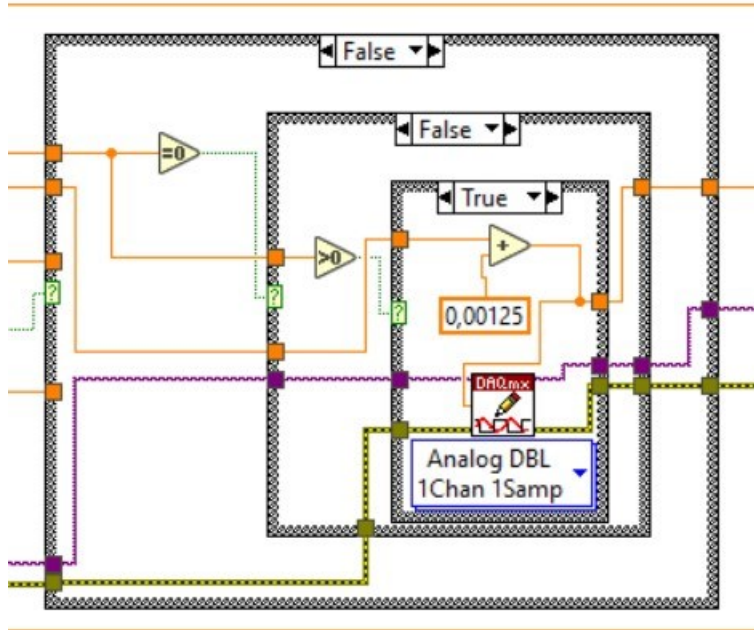

Figure 39. Detail of block diagram of the devised real-time LabVIEW program. The depicted operation corresponds to that of figure 30.

Figure 40 presents the operation of the devised real-time LabVIEW program in a situation where there is fluctuation in the measured output voltage value, and it is determined that the reference voltage needs to be decreased in order to approach the maximum power point.
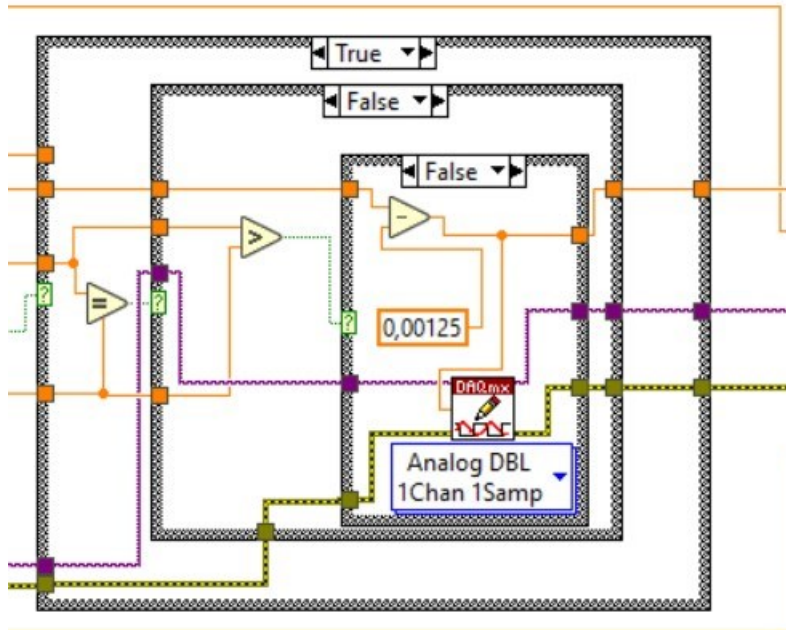
Figure 40. Detail of block diagram of the devised real-time LabVIEW program. The depicted operation corresponds to that of figure 31.

Another condition, namely one where the reference voltage needs to be increased in order to approach the maximum power point amidst fluctuation in the measured output voltage, is illustrated in figure 41.
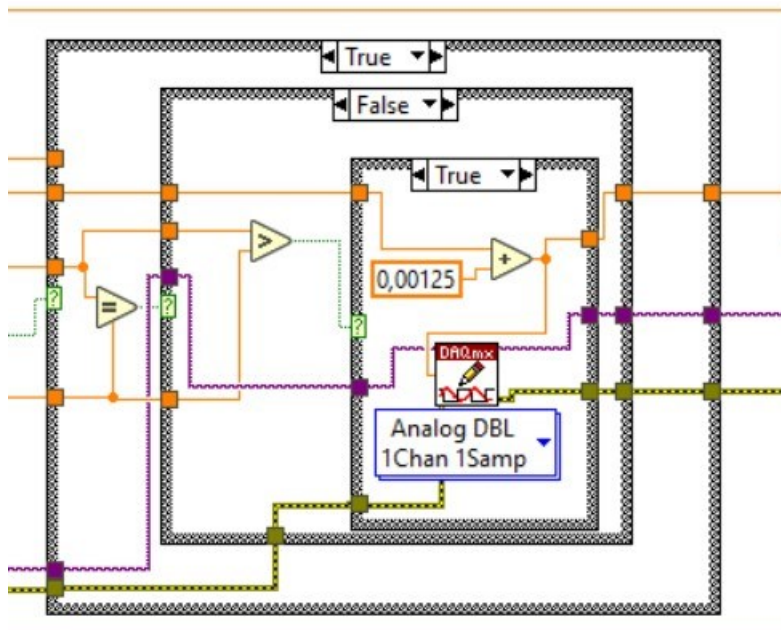

Figure 41. Detail of block diagram of the devised real-time LabVIEW program. The depicted operation corresponds to that of figure 32.

And finally, figure 42 illustrates the operation of the real-time LabVIEW program as the measured output voltage is fluctuating, but the system is determined to be already operating at the maximum power point.
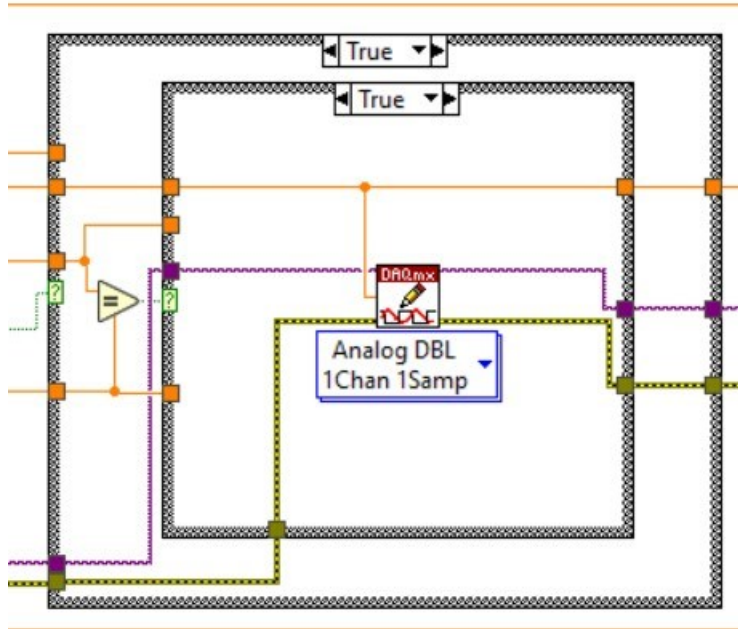

Figure 42. Detail of block diagram of the devised real-time LabVIEW program. The depicted operation corresponds to that of figure 33.

A real-time incremental conductance MPPT LabVIEW application seems relatively straightforward to program as well as quite feasible to implement in practice. Further refinements into the algorithm that would allow a global maximum power point to be reached in the operation of the system may prove to be very challenging to program, however.

7   Conclusion

It is rather obvious that manufacturing affordable and efficient solar energy solutions, presumably predominantly for small-scale off-grid applications, is a possible, yet complicated, task. The availability of powerful computation capabilities in microchips has considerably facilitated the wider adaptation of

this technology. The circuitry that is implemented to achieve these goals includes basic and well-established electrical applications, such as direct current to direct current voltage converters, often augmented by well-known computational algorithms such as MPPT. The technology already exists, so that no huge technological revolution is necessary in order to make efficient, affordable and environmentally sustainable energy production available to the general public.

In any case, there remain questions considering the relevance of general theory describing the operation of solar cells and solar panels when it comes to those aspects of the operation of these devices that will be the most relevant regarding practical real-world applications. As stated previously, the most commonly presented aspects of solar cells and solar panels are figures obtained at constant temperature and at constant irradiance. As such, they do not represent the real-world operating conditions of solar panels in, say, a small-scale off-grid system.

Furthermore, this creates issues regarding the computer simulation of such devices. While more than adequate computational models of both solar cells and solar panels are readily available, only a limited number of these models incorporate elements of environmental conditions. Considering the vast potential for efficient and reliable computer simulation of these systems, their design and testing need not only be a trial and error -based process involving whatever commercial solar panels can easily be obtained. Simulation as an integral part of the process of system design could result in major improvements in both environmental and economic feasibility.

References

1   Bureau of Naval Personnel. (1970). *Basic Electricity*. Second edition. Dover Books on Electrical Engineering. Garden City: Dover Publications.

2   Lee, HoSung. (2010). *Thermal Design. Heat Sinks, Thermoelectrics, Heat Pipes, Compact Heat Exchangers, and Solar Cells*. Hoboken: John Wiley & Sons, Inc.

3   Gitano-Briggs, Horizon. (2010). Small Wind Turbine Power Controllers. In Muyeen, S. M. (Ed.): *Wind Power*. 165-188. London: InTech Open.

4   Messenger, Roger A. & Ventre, Jerry. (2010*). Photovoltaic Systems Engineering*. Third edition. Boca Raton: CRC Press.

5   Su, Q. et al. (2010). Green Solar Electric Vehicle Changing the Future Lifestyle of Human In: *World Electric Vehicle Journal*. Volume 4 (1). 128-132.

6   PVEducation. *IV Curve* [WWW document] https://www.pveducation.org/pvcdrom/solar-cell-operation/iv-curve (Accessed June 5, 2022)

7   Eicker, Ursula. (2003). *Solar Technologies for Buildings*. Chichester: Wiley.

8   Hansen, Clifford W. (2015). *Parameter Estimation for Single Diode Models of Photovoltaic Modules*. Sandia Report SAND2015-2065. Albuquerque: Sandia National Laboratories.

9   National Instruments. (2014). *New Models for Photovoltaic Cells in Multisim* [WWW document] https://forums.ni.com/t5/NI-Circuit-Design-Community-Blog/New-Models-for-Photovoltaic-Cells-in-Multisim/ba-p/3473652?profile.language=en (Accessed June 5, 2022)

10   National Instruments. (2017). *Solar Panel Equivalent Circuit* [WWW document] https://www.multisim.com/content/EiUYiEGuC9bzrT2BAJto5f/solar-panel-equivalent-circuit/ (Accessed June 5, 2022)

11   TikZBlog. (2021). *How to draw a DC/DC Buck Converter in LaTeX using CircuiTikZ* [WWW document] https://latexdraw.com/dc-dc-buck-converter-latex-circuitikz/ (Accessed June 6, 2022)

12   Cordell, Bob. (2010). *Designing Audio Power Amplifiers*. New York: McGraw-Hill.

13 Shaharuddin, Ahmad & Ghani, Rasli. (2014). Modelling and Simulation of Boost Converter with Maximum Power Point Tracking (MPPT) for Photovoltaic Application In: *Jurnal Teknologi*. Volume 71 (5). 1-4.

14 Mühendis, Abdulkadir & Kulaksiz, Ahmet Afşin. (2020). LabVIEW Based Modeling System Applied in Maximum Power Point Tracking Techniques. *1st International Conference on Computer, Electrical and Electronics Sciences*. Konya, Turkey. October 8–10, 2020.

15 Lokanadham, M. & Vijaya Bhaskar, K. (2012). Incremental Conductance Based Maximum Power Point Tracking (MPPT) for Photovoltaic System In: *International Journal of Engineering Research and Applications (IJERA)*. Volume 2 (2). 1420-1424.

16 Srinivas, P., Vijaya Lakshmi, K., & Ramesh, Ch. (2016). Simulation of Incremental Conductance MPPT Algorithm for PV Systems using LabVIEW In: *International Journal of Innovative Research in Electrical, Electronics, Instrumentation and Control Engineering*. Volume 4 (1). 34-38.

17 Velkovski, Bodan & Pejovski, Dejan. (2016). Application of Incremental Conductance MPPT Method for a Photovoltaic Generator in LabVIEW. *20th International Student Conference on Electrical Engineering*. Prague, Czech Republic. May 24, 2016.

18 LTC6992-1/LTC6992-2/LTC6992-3/LTC6992-4 TimerBlox: Voltage-Controlled Pulse Width Modulator (PWM). Analog Devices. November 2019.

19 Analog Devices. *LTC6992 Voltage-Controlled Pulse Width Modulator* [WWW document] http://beta-tools.analog.com/timerblox/LTC6992 (Accessed May 26, 2022)

20 Openlabpro. *Pulse Width Modulation* [WWW document] https://openlabpro.com/guide/pulse-width-modulation/ (Accessed May 16, 2022)